Cell Reports
Article

A Synthetic Lethal Interaction between APC/C and Topoisomerase Poisons Uncovered by Proteomic Screens

Manuel Eguren,[1] Mónica Álvarez-Fernández,[1] Fernando García,[2] Andrés J. López-Contreras,[3] Kazuyuki Fujimitsu,[4] Hiroko Yaguchi,[4] José Luis Luque-García,[5] Oscar Fernández-Capetillo,[3] Javier Muñoz,[2] Hiroyuki Yamano,[4] and Marcos Malumbres[1,*]

[1]Cell Division and Cancer Group, Spanish National Cancer Research Centre (CNIO), Madrid 28029, Spain
[2]Proteomics Unit, Spanish National Cancer Research Centre (CNIO), Madrid 28029, Spain
[3]Genomic Instability Group, Spanish National Cancer Research Centre (CNIO), Madrid 28029, Spain
[4]Cell Cycle Control Group, University College London Cancer Institute, London WC1E 6BT, UK
[5]Department of Analytical Chemistry, Complutense University of Madrid, Madrid 28015, Spain
*Correspondence: malumbres@cnio.es
http://dx.doi.org/10.1016/j.celrep.2014.01.017

SUMMARY

The Anaphase-promoting complex/cyclosome (APC/C) cofactor Cdh1 modulates cell proliferation by targeting multiple cell-cycle regulators for ubiquitin-dependent degradation. Lack of Cdh1 results in structural and numerical chromosome aberrations, a hallmark of genomic instability. By using a proteomic approach in Cdh1-null cells and mouse tissues, we have identified kinesin Eg5 and topoisomerase 2α as Cdh1 targets involved in the maintenance of genomic stability. These proteins are ubiquitinated and degraded through specific KEN and D boxes in a Cdh1-dependent manner. Whereas Cdh1-null cells display partial resistance to Eg5 inhibitors such as monastrol, lack of Cdh1 results in a dramatic sensitivity to Top2α poisons as a consequence of increased levels of trapped Top2α-DNA complexes. Chemical inhibition of the APC/C in cancer cells results in increased sensitivity to Top2α poisons. This work identifies in vivo targets of the mammalian APC/C-Cdh1 complex and reveals synthetic lethal interactions of relevance in anticancer treatments.

INTRODUCTION

The eukaryotic cell cycle is tightly regulated through the control of the protein level and activity of critical enzymes. The Anaphase-promoting Complex/Cyclosome (APC/C) is a multimeric complex that ubiquitinates and targets for degradation multiple cell-cycle regulators (Peters, 2006). The temporal activities of the APC/C require two subunits, called cofactors, which bind and activate this complex at different times. Cdc20 activates the APC/C during mitosis targeting securin and mitotic cyclins for degradation, thus triggering mitotic exit. Cdh1, on the other hand, replaces Cdc20 during mitotic exit and targets multiple cell-cycle regulators for degradation, thus preventing unscheduled entry into S phase and replicative stress (Eguren et al., 2011; Peters, 2006). Whereas Cdc20 is essential for the metaphase-to-anaphase transition (Manchado et al., 2010b), Cdh1 is dispensable for cell-cycle progression from yeast to mammals (García-Higuera et al., 2008). Yet, lack of mammalian Cdh1 results in pleiotropic defects that include early entry into S phase, defective chromosome segregation, and accumulation to polyploid cells, as well as chromosomal and genomic instability (García-Higuera et al., 2008; Li et al., 2008; Sigl et al., 2009).

Whereas Cdc20 is able to target only a reduced number of proteins for degradation, the activity of Cdh1 is much more promiscuous. Known Cdh1 substrates include proteins involved in mitosis and cytokinesis (A- and B-type cyclins, Aurora A and B, Tpx2, Plk1, etc.), DNA replication (geminin, thymidine kinase 1, and thymidylate kinase), neuron biology, metabolism, etc. (Eguren et al., 2011; Manchado et al., 2010a; Peters, 2006). Despite the relevance of Cdh1 as a major regulator of the cell cycle and a critical modulator of cellular transformation, it is not currently clear which Cdh1 substrates mediate genomic instability or how the defects found in Cdh1-deficient tumor cells can be manipulated for therapeutic intervention in cancer. We have used Cdh1-null cells and mice (García-Higuera et al., 2008) to perform an unbiased analysis of proteins upregulated in the absence of this APC/C cofactor. Among these proteins, we describe here the relevance of Eg5 and Top2α, two targets of interest in cancer therapy. These two proteins are significantly upregulated in the absence of Cdh1, in vitro and in vivo, and are ubiquitinated in an APC/C-Cdh1-dependent manner. In addition, upregulation of these targets in Cdh1-deficient cells results in differential responses (increased resistance or susceptibility) to specific therapeutic agents, thus highlighting the clinical relevance of these findings.

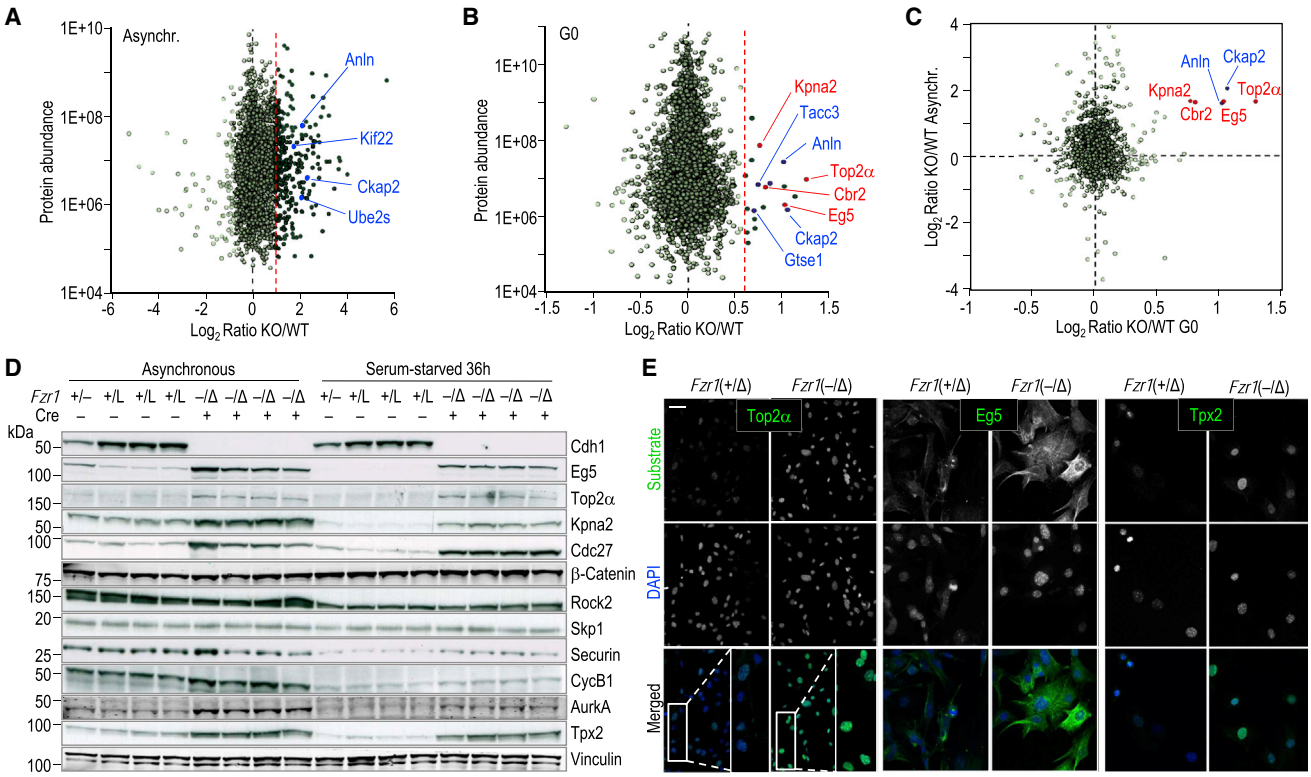

Figure 1. Quantitative Proteomics in Cdh1-Null Mouse Embryonic Fibroblasts

(A) The levels of proteins were compared in immortal *Fzr1*(–/–) or wild-type cells with SILAC. The protein ratios between the heavy (Cdh1-null cells) and light (wild-type cells) labeled samples are plotted against their protein abundance (estimated as average area of the three unique peptides with the largest peak area per protein; see Figure S1). Significantly upregulated known substrates are indicated in blue.

(B) iTRAQ analysis in serum-starved MEFs. The ratio between protein levels in *Fzr1*(–/–) and *Fzr1*(+/+) MEFs is shown in the x axis as a function of their abundances. Known mammalian substrates are indicated in blue, whereas additional proteins upregulated both in asynchronous and serum-starved cultures are shown in red.

(C) Correlation between the protein accumulation in asynchronous cultures (y axis) and serum-starved cells (x axis). Known mammalian substrates are indicated in blue, whereas hits upregulated in both studies are shown in red.

(D) Protein levels of known Cdh1 substrates (Aurora A, Tpx2, Securin, Cyclin B1) and additional hits found in our previous proteomics analyses. *Fzr1*(+/–) are heterozygous MEFs carrying a normal allele and a germline, null allele. *Fzr1*(+/L) carry a lox (L) allele that normally expresses Cdh1. This allele results in a null allele [*Fzr1*(Δ)] after expression of the recombinase Cre.

(E) Protein levels of Eg5 and Top2α in Cdh1-null [*Fzr1*(–/Δ)] and control heterozygous [*Fzr1*(+/Δ)] MEFs as detected by immunofluorescence. Tpx2 was used as a control. Scale bars, 50 μm.

RESULTS

Quantitative Proteomics Screens in Cdh1-Null Cells

We first analyzed the relative amount of proteins in the absence of Cdh1 by stable isotope labeling with amino acids in cell culture (SILAC; see the Experimental Procedures; Figure S1). We differentially labeled Cdh1- (encoded by the *Fzr1* locus in mammals) deficient [*Fzr1*(–/–); (García-Higuera et al., 2008)] mouse embryonic fibroblasts (MEFs) and their control [*Fzr1*(+/+)] cultures with heavy or light isotopes, respectively. Asynchronous cultures (Figure S2) were harvested, and proteins were quantified by mass spectrometry. Overall, we were able to obtain quantitative measurements for 2,324 proteins, from which 308 showed upregulation in the absence of Cdh1 (protein $\log_2$ ratio >1; equivalent to 2-fold; Figure 1A). Among them, we found known APC/C-Cdh1 substrates such as Anillin, Kif22, Ube2s, or Ckap2.

Because lack of Cdh1 may result in shorter G1 and longer S phase (Figure S2; García-Higuera et al., 2008; Sigl et al., 2009), we complemented these studies with protein profiles obtained 36 hr after removal of serum, a time in which both wild-type and Cdh1-null cells are quiescent (Figure S2) and known substrates accumulate in the absence of Cdh1 (García-Higuera et al., 2008). The corresponding protein lysates were then analyzed by using the isobaric tag for relative and absolute quantitation (iTRAQ) technique. The relative levels of 4,198 proteins were quantified, and 21 proteins were upregulated ($\log_2$ ratio >0.58; equivalent to 1.5-fold) in these Cdh1-null serum-starved cultures including known mammalian substrates of the APC/C complex, such as Anillin, Tacc3, Ckap2, or Gtse1. Additional hits that were also upregulated in the previous analysis in asynchronous cultures (Figure 1A) include Eg5, Top2α, Cbr2, or Kpna2 (Figures 1B and 1C). The differential expression of several of these proteins was validated by immunodetection in lysates

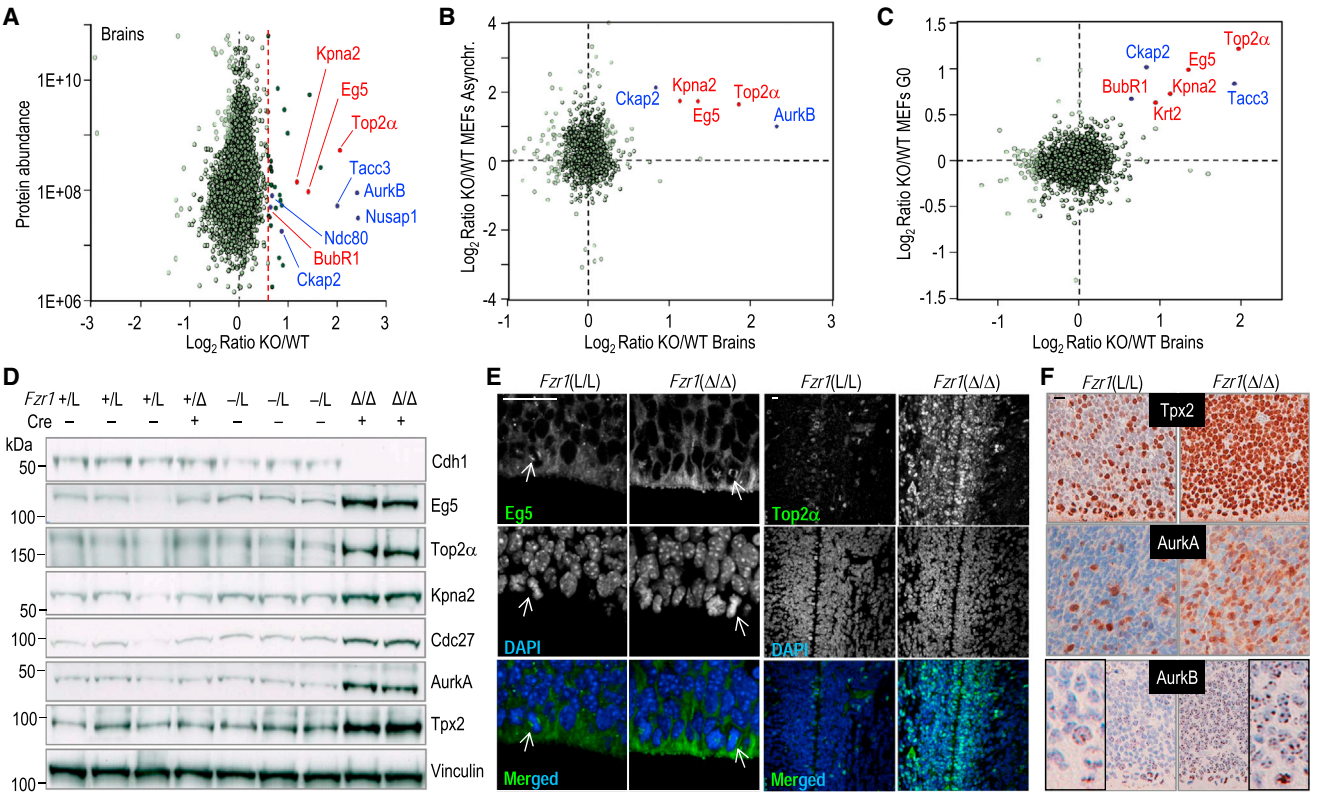

Figure 2. Quantitative Proteomics Screens in Cdh1-Deficient Brains

(A) The ratio between protein levels in *Fzr1*(–/Δ) and *Fzr1*(+/Δ) brains is shown in the x axis against the estimated protein abundance (see also Figure S1).

(B) Correlation between the data from asynchronous cultures in MEFs (y axis) and data in brains (x axis).

(C) Correlation between the data from serum-starved MEFs (y axis) and embryonic brains (x axis). In (A)–(C), known substrates are indicated in blue, whereas additional proteins upregulated both in MEFs (Figure 1) and brains are shown in red.

(D) Protein levels of molecules found in the proteomics screens in Cdh1-null [*Fzr1*(Δ/Δ)], heterozygous [*Fzr1*(+/Δ) and *Fzr1*(–/L)], and normal [*Fzr1*(+/L)] E15.5 brains. Known Cdh1 substrates (Aurora A, Tpx2) and control panels are taken from Eguren et al. (2013) with permission.

(E) Immunofluorescence of Eg5 and Top2α in Cdh1-null [*Fzr1*(Δ/Δ)] and control [*Fzr1*(L/L)] brains.

(F) Immunohistochemistry analysis of known Cdh1 targets (Tpx2, Aurora A and Aurora B) in Cdh1-null [*Fzr1*(Δ/Δ)] and control [*Fzr1*(L/L)] brains. Nuclei were counterstained with hematoxylin. Scale bars, 25 μm.

from Cdh1-null and control fibroblasts (Figure 1D). The upregulation of two of these candidates, Eg5 and Top2α, was also validated by immunofluorescence in cultured MEFs (Figure 1E).

We next tested the differential expression of proteins in vivo by using Cdh1-deficient brains, a tissue in which ablation of the Cdh1-encoding gene, *Fzr1*, results in developmental defects (Eguren et al., 2013). Given that Cdh1 is essential for endoreplication in placental trophoblast giant cells, we used *Sox2-Cre* mice to specifically ablate Cdh1 in the embryo but not in placental tissues (García-Higuera et al., 2008). Brains from embryonic day (E)15.5 *Fzr1*(–/Δ); *Sox2-Cre* and control embryos were differentially labeled with iTRAQ reagents and analyzed by mass spectrometry (Figure S1). This analysis provided quantitative data for 3,466 proteins, from which 31 were upregulated more than 1.5-fold ($\log_2$ ratio > 0.58) in Cdh1-null brains, including the known substrates Tacc3, Aurora B, Nusap1, Ndc80, and Ckap2 (Figure 2A). Interestingly, three of the most differentially expressed proteins found in Cdh1-null MEFs, Eg5, Top2α, and Kpna2 were also upregulated in Cdh1-null brains (Figures 2A–2C). These results were validated by immunoblot (Figure 2D) or immunofluorescence (Figures 2E and 2F) analysis using brains from different E14.5–16.5 Cdh1-null and control embryos.

Nine proteins were found consistently upregulated in the three different systems (asynchronous MEFs, serum-starved MEFs, and embryonic brains) or were upregulated in two of them and not detected in the third one (Table 1). This set of nine proteins was enriched in known mammalian Cdh1 substrates (3/9 = 33% versus 29 known substrates [Table S1] among the 5,997 proteins [0.5%] analyzed in this study; $p < 0.001$). Some other known substrates were only upregulated or detected in one of the three studies or were not upregulated (Table S1). In addition, five of the proteins selected in Table 1 contain KEN boxes (56% versus 11% in the 5,997 proteins identified in these studies; $p < 0.0001$). Four of them (44%) also contained a D box as defined by the R-X-X-L-X-[LIVM] sequence, although this percentage was not significantly different from that found in the whole set of proteins analyzed (46%). On the other hand, all these nine proteins

Table 1. Proteins Significantly Upregulated in at Least Two of the Three Proteomics Screens in Cdh1-Deficient Cells[a]

Symbol	Uniprot	Description	Log_2 KO/WT Async. MEFs	Log_2 KO/WT G0 MEFs	Log_2 KO/WT Brains	KEN[b]	D Box[c]	RXXL[d]	Reference
Top2α	Q01320	DNA topoisomerase 2-alpha	1.584	1.222	2.01	1	2	5	
Kif11	Q6P9P6	Kinesin-like protein KIF11 (Eg5)	1.72	0.996	1.374	1	—	3	
Ckap2	Q3V1H1	Cytoskeleton-associated protein 2	2.116	1.024	0.845	1	—	2	Hong et al., 2007; Seki and Fang, 2007
Kpna2	P52293	Importin subunit alpha-2	1.729	0.737	1.145	—	—	2	
Tacc3	Q9JJ11	Transforming acidic coiled-coil-containing protein 3	ND	0.845	1.959	2	—	2	Jeng et al., 2009
Anln	Q8K298	Actin-binding protein anillin	1.668	0.983	ND	—	3	11	Zhao and Fang, 2005
Cbr2	P08074	Carbonyl reductase [NADPH] 2	1.696	0.774	ND	—	—	1	
Krt2	Q3TTY5	Keratin, type II cytoskeletal 2 epidermal	ND	0.66	0.977	—	2	3	
BubR1	Q9Z1S0	Mitotic checkpoint serine/threonine-protein kinase BUB1 β	ND	0.683	0.655	2	3	7	

ND, not detected.
[a]Known candidates are accompanied by the corresponding references.
[b]The number of KEN boxes (K-E-N).
[c]The number of D boxes (R-X-X-L-X-[LIVM]) as defined in the Eukaryotic Linear Motif resource (http://elm.eu.org/).
[d]The number of relaxed D boxes (R-X-X-L). The presence of these three domains (KEN, D box, and RXXL) was analyzed with ScanProsite (http://prosite.expasy.org/scanprosite/).

(100% versus 83% in the set of 5,997 proteins; $p < 0.001$) contain a relaxed D box as defined by the R-X-X-L sequence (Table 1).

Cdh1 Controls the Protein Levels of Eg5 and Top2α in Mouse and Human Cells

We next tested the effect of Cdh1 overexpression or downregulation in human cells. Human 293T cells were transfected with vectors expressing Cdc20, Cdh1, or a hyperactive Cdh1 mutant ($Cdh1^{ALA}$) carrying nine mutations that make this protein insensitive to its inhibition by Cdk-dependent phosphorylation (Kramer et al., 2000). As shown in Figure 3A, expression of either Cdh1 or $Cdh1^{ALA}$ resulted in downregulation of Eg5, Top2α, as well as known Cdh1 substrates. These differences were not due to changes in cell-cycle profile because overexpression of these APC/C cofactors did not change DNA content in these cultures (Figure S2). In these assays, Cdc20 induced downregulation of its substrate securin, but not the other molecules. On the other hand, knockdown of Cdh1 in human cells resulted in increased levels of Eg5 and Top2α, similarly to known substrates such as Tpx2 and Aurora A (Figure 3B). The upregulation of Eg5 and Top2α in Cdh1-null cells was not a consequence of increased transcription because the levels of the corresponding transcripts were not increased (Figure 3C). These mutant cells, however, displayed a significant transcriptional upregulation of $p21^{Cip1}$ and Gadd45a, in agreement with the DNA-damage-like response in these cells and their increased susceptibility to become senescent (Eguren et al., 2013; García-Higuera et al., 2008; Li et al., 2008). Both Eg5 and Top2α were unstable proteins after the inhibition of protein synthesis with cycloheximide (Figure 3D) or actinomycin D (Figure S2). Importantly, the levels of these two proteins, similarly to Aurora A, were partially stabilized in Cdh1-null cells. Reintroduction of exogenous Cdh1 in *Fzr1*(–/–) cells restored the levels of Eg5 and Top2α, and this was dependent on the proteasome (Figure 3E). Finally, coimmunoprecipitation studies indicated that Cdh1 was able to bind both Eg5 (Figure 3F) and Top2α (Figure 3G), supporting a role for APC/C-Cdh1 in the degradation of these two proteins.

We then tested the direct ubiquitination of these two proteins by APC/C-Cdh1 complexes using cell-free ubiquitination and destruction assays in *Xenopus* egg extracts. As shown in Figures 3H and S3, Eg5 was ubiquitinated and degraded after the addition of recombinant Cdh1 protein in these assays. Both Cdh1-dependent ubiquitination and degradation were prevented after mutagenesis of a KEN box sequence (amino acids [aa] 1,022–1,024 in the human Eg5 sequence) and two D box sequences (aa 944–947 and 1,047–1,050; Figure S3). Accordingly, the Eg5 isoform carrying these three mutations (Eg5_3M) was unable to efficiently bind Cdh1 (Figure S3). Top2α was not efficiently degraded in a similar assay in *Xenopus* egg extracts (Figure 3I). However, Top2α was ubiquitinated in a Cdh1-dependent manner following a similar kinetics to that observed for Eg5, and its ubiquitination was lost in a Top2α mutant carrying specific mutations in a KEN box (aa 378–380) and two putative D boxes (aa 982–985 and 1,053–1,056 in the human sequence; Figure 3I and S3). These data suggest that both Eg5 and Top2α are ubiquitinated in a Cdh1-dependent manner.

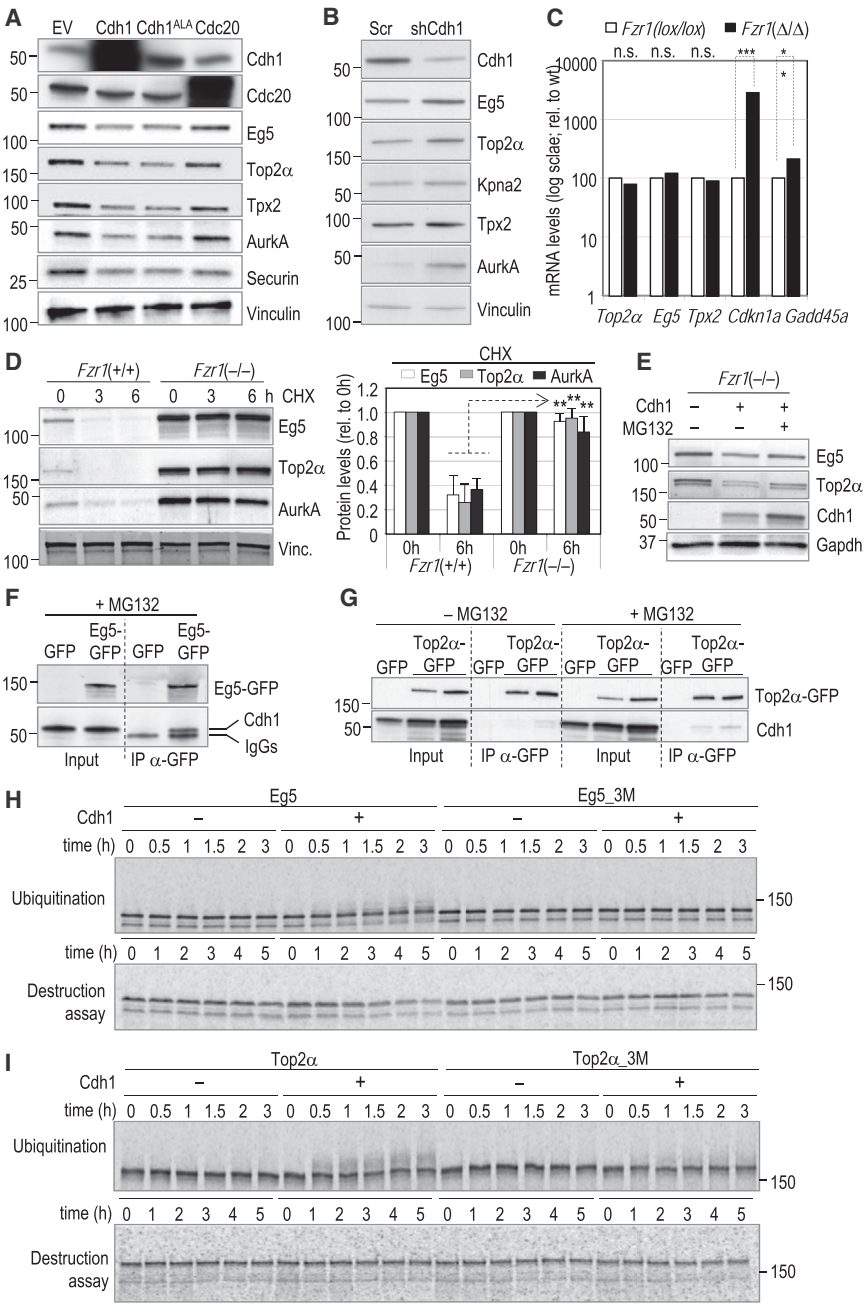

Figure 3. Cdh1 Controls Eg5 and Top2α Protein Stability

(A) Protein levels of the indicated molecules after overexpression of Cdh1 (wild-type form or the $Cdh1^{ALA}$ constitutive active mutant) or Cdc20 in human 293T cells.

(B) Protein levels of the indicated molecules 72 hr after transfection of 293T cells with a short hairpin RNA against Cdh1 or against scrambled (Scr.) sequences.

(C) Quantification (log_{10} scale) of mRNA levels of the indicated transcripts by real-time RT-PCR. *Cdkn1a* is the symbol of the locus encoding the p53-responsive cell-cycle inhibitor $p21^{Cip1}$.

(D) Protein stability of the indicated molecules in the presence of cycloheximide (CHX) in Cdh1-null and control cells. The quantification of protein levels (mean ± SEM) at 0 and 6 after the addition of CHX is shown.

(E) Protein levels of the indicated molecules after expression of Cdh1 in *Fzr1*(–/–) MEFs in the presence or absence of the proteasome inhibitor MG132.

(F and G) Coimmunoprecipitation studies in 293T cells transfected with Eg5 (F) or Top2α (G) -GFP fusion proteins. Protein extracts were immunoprecipitated with antibodies against GFP (α-GFP), and the endogenous Cdh1 was detected in the absence or presence of the proteasome inhibitor MG132.

(H) Cdh1-dependent ubiquitination and destruction of Eg5. ^{35}S-labeled wild-type or triple mutant (3M; see Figure S3) Eg5 were subjected to an in vitro ubiquitination assay using purified *Xenopus* APC/C in the presence or absence of Cdh1 (upper panel) or a cell-free destruction assay reconstituted in *Xenopus* egg interphase extracts in the presence or absence of Cdh1 (lower panel).

(I) Similar ubiquitination and destruction assays with wild-type or triple mutant (3M) Top2α. These blots are representative of three different assays.

Cdh1-Dependent Degradation of Eg5 and Top2α Contributes to Genomic Stability

We first synchronized MEFs in prometaphase by releasing these cells from double thymidine block in the presence of taxol. Mitotic cells were then selected by shake-off, plated in the absence of taxol, and harvested at different time points for protein analysis. Endogenous Eg5 was degraded during mitotic exit with a kinetics similar to that of known APC/C-Cdh1 substrates such as Tpx2 or Aurora kinase B, and slower than APC/C-Cdc20 substrates such as cyclin B1 or securin (Figures 4A and 4B). Importantly, the levels of all these substrates were stabilized during mitotic exit in Cdh1-null cells (Figures 4A and S3). Mutation of the KEN box partially stabilized Eg5 during mitotic exit in a similar experimental setting, and this effect was further enhanced upon mutation of the two putative D boxes present in this protein (Figure S3). Time-lapse studies in NIH 3T3 cells also showed that Eg5 is degraded during telophase and maintained at low levels during the following G1 phase, whereas the levels of the triple mutant (Eg5_3M) remained high in the cytoplasm of interphasic cells (Figures 4C and 4D). Similar assays indicated that Top2α was degraded in a gradual manner after mitotic exit, and most of its degradation occurred after several hours in G1. Importantly, the Top2α_3M mutant displayed a significant stabilization (Figures 4C and 4D) in agreement with a role for the APC/C-Cdh1 recognition sites in the degradation of this molecule.

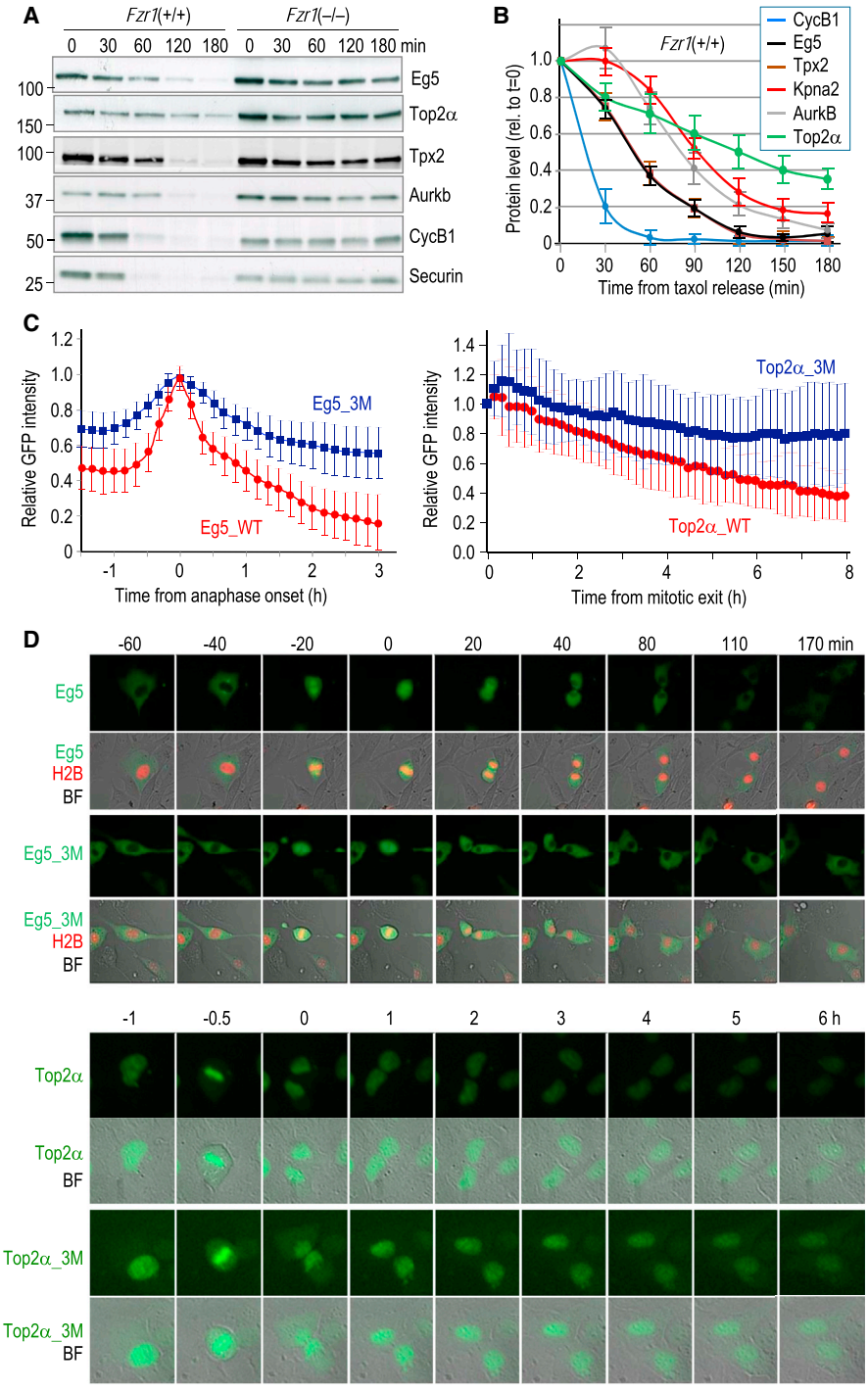

Figure 4. Degradation of the Kinesin Eg5 during Mitotic Exit

(A) Protein levels of the indicated molecules at different time points after a release from taxol.

(B) Comparative profiles of the levels (mean ± SEM) of the indicated proteins after release from taxol from three different assays. Values are normalized to the amount of protein at t = 0 (in the presence of taxol).

(C) Quantification of the degradation of Eg5- or Top2α-GFP fusion proteins during mitotic exit (after anaphase onset or DNA decondensation) as monitored by videomicroscopy. The quantification shows the comparative levels of normal Eg5 or the Eg5_3M mutant (n = 16 cells; left panel) or wild-type Top2α or the Top2α_3M mutant (n = 10 cells; right panel). Cells were aligned in metaphase for Eg5 or telophase upon DNA decondensation for Top2α (t = 0), and the intensity (mean ± SD) of the signal was arbitrarily set as 1.

(D) Representative images of mitotic progression in the presence of Eg5, Eg5_3M, Top2α, or Top2α_3M (green) GFP fusion proteins. The signal of a histone H2B-mCherry fusion protein is in red. BF, bright field. Time 0 indicates anaphase onset (top) or mitotic exit (bottom panels). Scale bars, 25 μm.

Overexpression of either of these molecules resulted in increased DNA damage (as scored by the number of 53BP1 foci; Figure S4). Overexpression of Eg5 also resulted in abnormal mitotic figures characterized by lagging chromosomes and anaphase bridges. These abnormalities were also present after overexpression of Top2α although the increase in mitotic aberrations was not statistically significant in our assays. These abnormal figures were also frequent in Cdh1-null cells, and knockdown of either Eg5 or Top2α partially rescued these aberrations (Figure S4), suggesting that the increased levels of Eg5 and Top2α may contribute to the genomic alterations (DNA damage and mitotic aberrations) found in Cdh1-null cells.

Cdh1-Dependent Degradation of Eg5 Modulates the Response to Eg5 Inhibitors

Pioneer screens to identify antimitotic drugs led to the characterization of monastrol as an Eg5 inhibitor (Mayer et al., 1999), and several Eg5 inhibitors are now in clinical trials (Doménech and Malumbres, 2013; Rath and Kozielski, 2012). Treatment with monastrol leads to a mitotic-checkpoint-dependent mitotic arrest and lack of chromosome segregation due to the lack of a bipolar spindle. However, Cdh1-null cells displayed partial resistance to monastrol as chromosome segregation occurred in more than 20% of these mutant cells in the presence of similar levels of this drug (Figures 5A, 5B, and S5). Importantly, this resistance was likely to be due to the increased levels of Eg5 as concomitant downregulation of this protein using RNA interference completely prevented chromosome segregation in the presence of monastrol (Figures 5C and 5D). Parallel knockdown of Eg5 in untreated cells resulted in normal segregation in most cells, and only 15% of these treated cells displayed problems during mitosis. Knockdown of Eg5 restored susceptibility to monastrol in terms of chromosome segregation and also prevented the rapid exit from mitosis observed in a few (7%; n = 45) Cdh1-null cells treated with monastrol (Figures 5B and 5D). The resistance of Cdh1-null cells was less evident when using increasing concentrations of monastrol (Figure S5), suggesting a dosage effect in which Cdh1 inactivation leads to Eg5 overexpression, and this overexpression results in a partial resistance of monastrol. In addition, these effects were specific of the Eg5 inhibitor monastrol, given that similar studies in the presence of taxol showed no resistance to this microtubule poison in the absence of Cdh1 (Figure S5).

Genetic Ablation of Cdh1 Leads to Increased Susceptibility to Topoisomerase Poisons

Compounds that target topoisomerase II are classified into two main classes with different mechanism of action: topoisomerase poisons (e.g., etoposide), which target the Top2α-DNA complex after the topoisomerase has created the DNA double-stranded break (DSB), and topoisomerase catalytic inhibitors (e.g., ICRF-193), which target the ATPase domain and therefore prevent the breakage made by Top2α (Nitiss, 2009). In fact, catalytic inhibitors are used to prevent some of the toxic effects of poisons, because they prevent the amount of DNA breakage in some sensitive organs such as the heart. Given that clinical data suggest that increased levels of Top2α correlate with the outcome of patients treated with topoisomerase inhibitors, we asked whether the increased levels of Top2α observed in Cdh1-deficient cells could modulate the sensitivity to the topoisomerase poison etoposide. Cdh1-deficient cells displayed a significant increase in the number of DNA breaks generated by etoposide as monitored by the nuclear staining of the phosphorylated form of histone H2AX (γH2AX; Figures 6A and S6). These data correlated with a dramatic increase in cell death after treatment of Cdh1-null cells with etoposide, as monitored by flow cytometry (Figure S6) or high-throughput microscopy (Figure 6B). For instance, about 70% of *Fzr1*(–/–) cells died after treatment with 25 μM etoposide, whereas less than 10% of control cells were killed in these conditions. No differences were observed in the response to the catalytic inhibitor ICR-193. However, this inhibitor was able to protect cells from the lethality observed after treatment with etoposide alone (Figure 6B), in agreement with the idea that DNA damage induced by topoisomerase poisons can be partially prevented by inhibiting the catalytic activity of these enzymes.

We then tested whether the susceptibility of Cdh1-null cells to etoposide is a consequence of increased Top2α expression. Overexpression of Top2α itself resulted in certain levels of DNA damage (Figures S4 and S6) and strongly cooperated with etoposide in inducing high levels of γH2AX (Figure S6). We then tried to rescue the damage in Cdh1-null cells by treating *Fzr1*(–/–) and control cells with etoposide or ICRF-193 in the presence of short hairpin RNA interfering molecules against Top2α transcripts or scrambled sequences. Two different small hairpin RNA (shRNA) sequences, #1284 and #2837, that display different efficiency in downregulating Top2α were used (Figure S4). Partial downregulation of Top2α with shTop2α #1284 resulted in a significant protection against the lethal effect of etoposide, and this effect was more dramatic when using sequence #2837, which is more effective knocking down Top2α (Figure 6C). It is important to note that, due to the high levels of upregulation of Top2α in Cdh1-null cells, these hairpin molecules were not able to modulate Top2α expression down to the levels found in wild-type cells (Figure S4), perhaps explaining that these rescued cells still displayed some sensitivity to etoposide (Figure 6C).

Chemical Inhibition of the APC/C Sensitizes Cells to Topoisomerase Poisons

Inhibition of the APC/C is currently considered as a therapeutic strategy in cancer by preventing Cdc20-dependent mitotic exit (Manchado et al., 2012). A small-molecule, proTAME, results in mitotic arrest in collaboration with microtubule poisons by inhibiting APC/C-Cdc20 complexes (Zeng et al., 2010). proTAME targets both APC/C-Cdc20 and APC/C-Cdh1 (Zeng et al., 2010), although the effect of inhibiting Cdh1 complexes has not been analyzed so far. As shown in Figure 7A, treatment of HeLa cells with different concentrations of proTAME resulted in increased levels of both Eg5 and Top2α in a dose-dependent manner. These differences were not due to mitotic arrest because the mitotic index of cells treated with 20 μM proTAME was 4.6% ± 1.1% compared to 2.1% ± 0.6% in untreated cultures. The upregulation of Top2α was also significant after immunofluorescence with specific antibodies, and these results

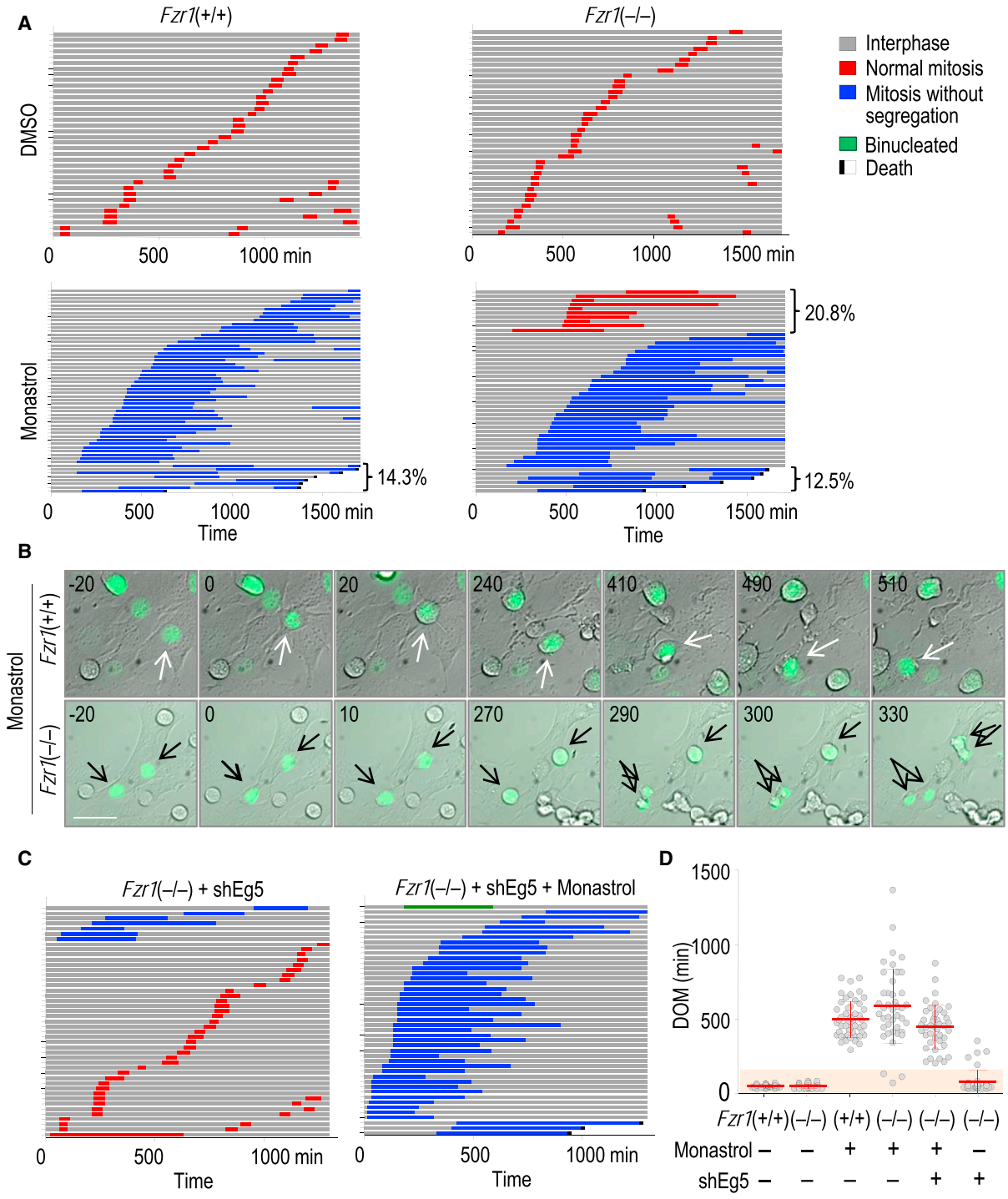

Figure 5. Absence of Cdh1 Results in Increased Resistance to Monastrol in an Eg5-Dependent Manner

(A) Plots showing the fate of individual Cdh1-null or control cells (rows) in the presence or absence of monastrol. The progression through interphase or abnormal or normal mitosis is represented as indicated. About 12%–14% of cells die in the presence of monastrol. One-fifth of Cdh1-null cells display chromosome segregation in the presence of monastrol, whereas this is not observed in wild-type cells (n = 45 cells per assay).

(B) Representative images of the effect of monastrol. This inhibitor prevents chromosome segregation in wild-type cells (top panels). Representative examples of Cdh1-null cells undergoing chromosome segregation are shown in the bottom panels. Time 0 indicates mitotic entry (chromosome condensation and rounding of cells). Histone H2B is in green. Scale bars, 25 μm.

(C) Effect of knockdown of Eg5 in Cdh1-null cells in the presence or absence of monastrol. Colors indicate cell fate as in (A). (n = 45 cells per assay.)

(D) Duration of mitosis (DOM) in the previous assays. Each dot corresponds to an individual cell (n = 45 cells per condition). Red bars indicate mean ± SD.

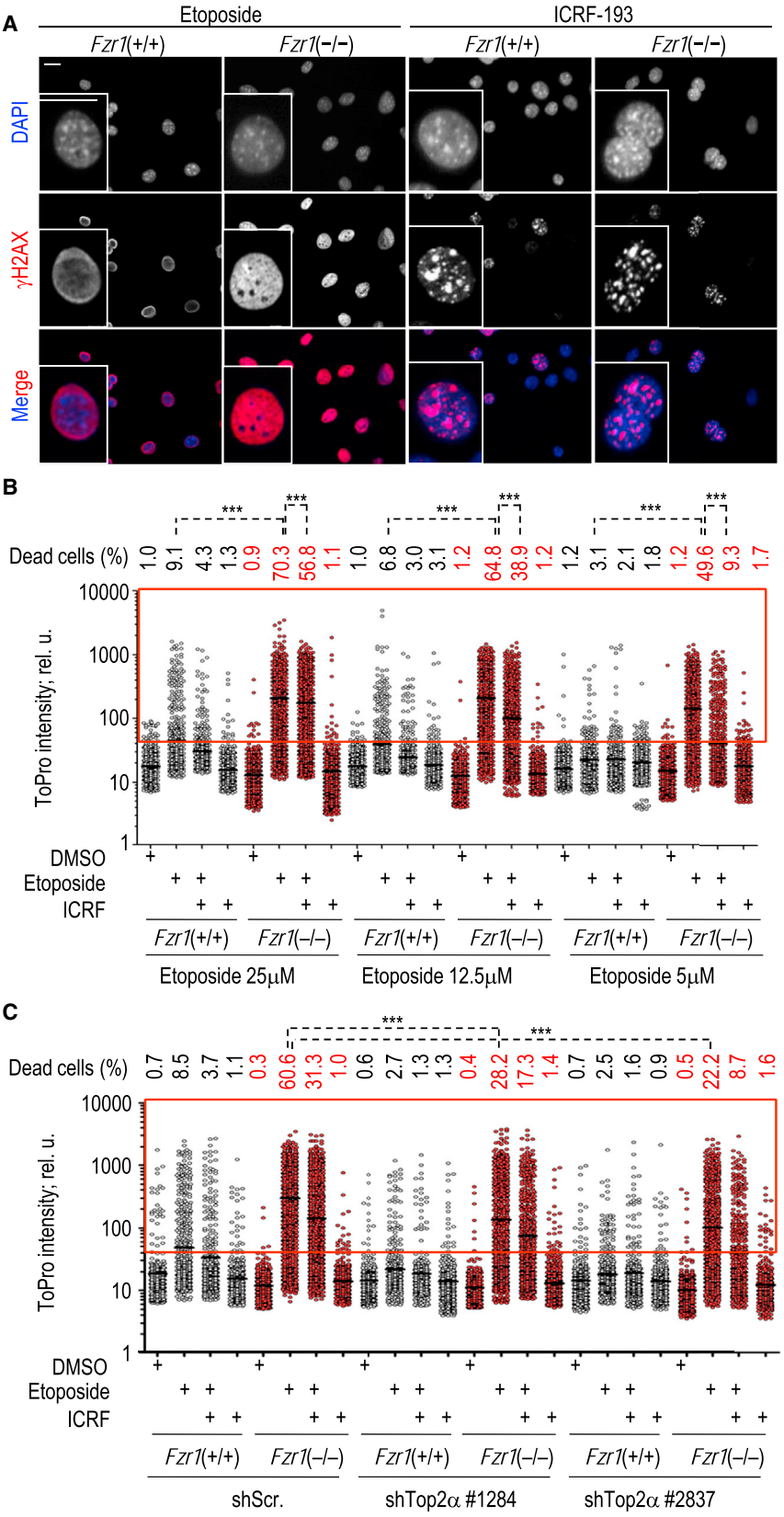

Figure 6. Effect of Topoisomerase Poisons and Catalytic Inhibitors in Cdh1-Deficient Cells

(A) DNA damage as monitored by phosphorylation of H2AX (γH2AX) induced by etoposide or ICRF-193 in Cdh1-null or control cells. Scale bars, 10 μm.

(B) Quantification of cell death by internalization of the dye TO-PRO using high-throughput microscopy. Cdh1-null (red) or control (black) cells were treated with etoposide (at the indicated doses) or ICRF-193 (5 μM). The percentage of dead cells (red frame) is indicated for each condition.

(C) Similar quantification of cell death after treatment with the indicated compounds and knockdown of Top2α using two different short hairpin interfering RNAs.

In (B) and (C), black horizontal bars indicate the mean. ***$p < 0.001$; Student's t test.

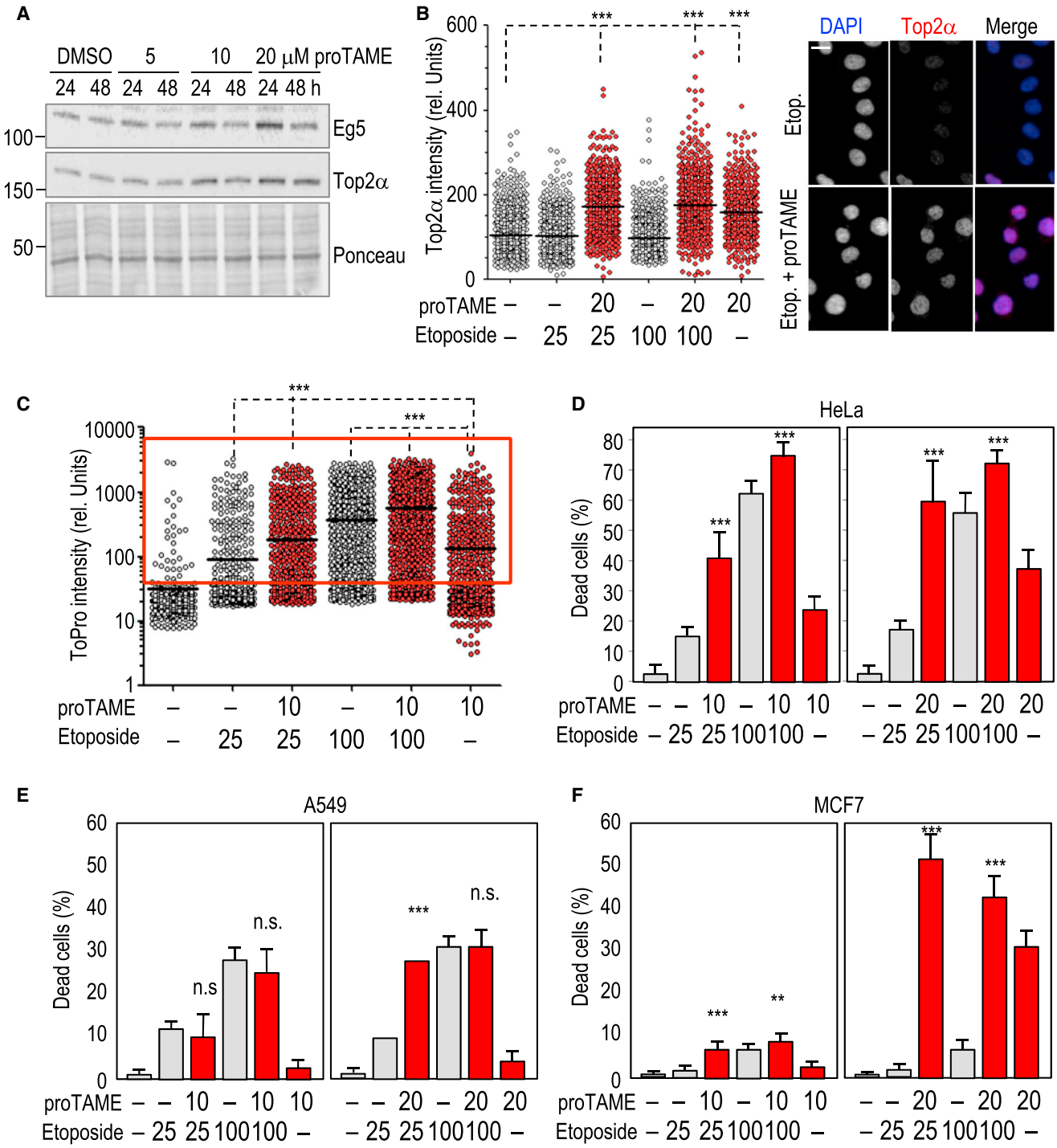

Figure 7. Cdh1 Inhibition Sensitizes Human Cancer Cells to Topoisomerase Poisons

(A) Protein levels of Eg5 and Top2α 24 or 48 hr after chemical inhibition of the APC/C using proTAME at the indicated dose in HeLa cells.

(B) Quantification of Top2α levels in HeLa cells treated with the indicated dose of proTAME or etoposide (μM). Horizontal bars indicate the mean. Representative images of cells treated with 25 μM etoposide or 25 μM etoposide + 20 μM proTAME. Top2α, red; DAPI, blue. Scale bars, 10 μM.

(C) Cellular intensity of the dye TO-PRO after treatment of HeLa cells with the indicated dose of proTAME or etoposide (μM). Mean is indicated as horizontal bars.

(D–F) Percentage of dead cells (mean, as considered in the frame shown in C ± SEM) after treatment of HeLa (D), A549 (E), or MCF7 (F) cells with the indicated dose of proTAME and etoposide (μM). At least 4,000 cells per condition were quantified in these assays (B–F), and only 1,000 are represented in (B) and (C) for clarity.

See Figure S7 for additional cell types. n.s., not significant; **p < 0.01; ***p < 0.001; Student's t test.

were also obtained in different cell types such as lung cancer cells (A549) and breast tumor cells (MCF7; Figure 7B and S7).

Importantly, inhibition of the APC/C with proTAME sensitized HeLa cells to etoposide. Whereas single treatment with proTAME or etoposide resulted in certain levels of lethality in HeLa cells, the combination of these two compounds resulted in a significant synergism, especially when low dose of proTAME was used (Figures 7C and 7D). In A549 cells, treatment with 10 μM of proTAME resulted in no dramatic differences in Top2α levels (Figure S7), and, accordingly, no differences in lethality were observed (Figure 7E). A combination of 20 μM of proTAME and 25 μM of etoposide resulted in a significant synergism in killing A549 cells, whereas higher concentrations of etoposide (100 μM) were not modulated by proTAME, suggesting that the combination of these two compounds is efficient in a specific window of moderate concentrations. Similarly, the synergism of this combination was evident using 10 μM of proTAME in MCF7 breast cancer cells, and much more dramatic when using 20 μM of this APC/C inhibitor in the presence of moderate concentrations of etoposide (Figure 7F). These concentrations of proTAME induced a dramatic upregulation of Top2α (Figure S7), suggesting that the therapeutic effect of this APC/C inhibitor correlates with its ability to induce Top2α accumulation.

DISCUSSION

We have made use of a combination of genetic and proteomic approaches to analyze major changes in protein levels in APC/C-Cdh1-deficient cells. Among the candidates, we have focused in this study in two molecules that scored among the highest accumulated proteins in three different proteomic analyses in Cdh1-null cells or tissues.

Eg5, also known as Kif11, is a bipolar, homotetrameric, plus-end-directed spindle motor protein of the kinesin-5 family involved in the proper formation of a bipolar spindle. Earlier work in budding yeast suggested that the related Cin8p and Kip1p kinesins are degraded in an APC/C-dependent manner. Cdc20-dependent degradation of Kip1p seems to depend on a 17 aa sequence with no primary homology to other known domains (Gordon and Roof, 2001), whereas degradation of Cin8p is Cdh1-dependent, although this protein also lacks a functional D box sequence (Hildebrandt and Hoyt, 2001). In mammals, overexpression of Eg5 results in mitotic defects in cultured cells (Figure S4) as well as genomic instability and tumor development in vivo (Castillo et al., 2007). In addition, this protein is commonly overexpressed in human tumors, and, given its function during mitotic progression, is currently under clinical evaluation as a cancer target (Doménech and Malumbres, 2013; Rath and Kozielski, 2012). Treatment of cells with the Eg5 inhibitor monastrol results in monopolar spindles and a mitotic arrest that depends on the activity of the mitotic checkpoint. Lack of Cdh1, however, results in partial resistance to monastrol, but not taxol, and this resistance is at least partially dependent on the increased Eg5 levels in these mutant cells. The correlation between Eg5 expression and the response to Eg5 inhibitors remains to be reported in clinical trials. Yet, Eg5 levels may correlate with the response to different antimitotic drugs combined with classical chemotherapies (Saijo et al., 2006).

The control of Eg5 by Cdh1 may also have additional clinical implications as the activity of this kinesin is also altered in human microcephaly (Ostergaard et al., 2012). In addition, Eg5 regulates axonal outgrowth (Myers and Baas, 2007; Nadar et al., 2008) and neuronal development (Ferhat et al., 1998) and migration (Falnikar et al., 2011). Inhibition of Eg5 is also currently considered as a strategy to improve axon regeneration (Haque et al., 2004; Lin et al., 2011). Importantly, Cdh1 has also been shown to be expressed in neural progenitors (Eguren et al., 2013) and post-mitotic neurons (Gieffers et al., 1999), regulates axonal growth (Konishi et al., 2004), and may be involved in neurodegenerative diseases in the mammalian brain (Aulia and Tang, 2006).

Proteomic analysis of Cdh1-null cells shows that Top2α is one of the most accumulated proteins in the absence of this APC/C cofactor (Figures 1 and 2). Top2α is known to be regulated by protein degradation although reported data suggest that this occurs in a Bmi1/Ring1A-dependent manner in the presence of DNA damage (Alchanati et al., 2009). Our data suggest that Top2α is ubiquitinated and degraded in a Cdh1-dependent manner during G1, and its ubiquitination and degradation can be prevented after mutation of specific KEN and D boxes (Figures 3 and 4). The kinetics of degradation of Top2α differs from other typical Cdh1 substrates in that this protein is degraded later in G1 rather than during mitotic exit (Figure 4; Heck et al., 1988; Tavormina et al., 2002), suggesting additional requirements that are unknown at this moment.

Topoisomerase poisons such as etoposide block the catalytic cycle after DNA is already cleaved by topoisomerase but before DNA religation, thus generating Top2-DNA covalent complexes. These poisons therefore convert Top2 into an agent that induces cellular damage (Nitiss, 2009). Cdh1-null cells are known to display high levels of DNA damage both in vitro (Sigl et al., 2009) and in vivo (Eguren et al., 2013). Lack of Cdh1 results in increased levels of Cyclin-Cdk activity and premature entry into S phase (García-Higuera et al., 2008), and partial inhibition of Cdk activity results in reduced replicative stress in Cdh1-null cells (Eguren et al., 2013). It is likely that the increased levels of Top2α in Cdh1-null cells contribute not only to the increased sensitivity to etoposide (Figures 6 and 7), but also to the DNA damage and genomic instability observed in the absence of this APC/C cofactor. Whereas Top2α is the main topoisomerase isoform expressed in proliferating cells, a switch in the protein levels from Top2α to Top2β occurs during neuronal differentiation (Tiwari et al., 2012; Watanabe et al., 1994). We have recently observed that lack of Cdh1 in the nervous system results in accumulation of γH2AX signal, defective development of the nervous system, and hydrocephalus (Eguren et al., 2013), suggesting that the control of Top2α levels by APC/C-Cdh1 may have a critical role during brain development.

The especial sensitivity of Cdh1-deficient cells to topoisomerase poisons may also have relevant implications in cancer therapy. Cdh1 targets for degradation many proteins involved in cell-cycle progression, and some of its substrates display oncogenic potential (Malumbres and Barbacid, 2009). Partial inactivation of Cdh1 results in increased susceptibility to tumor formation in mouse models (García-Higuera et al., 2008). The status of Cdh1 in human tumors has not been explored in detail. However, Cdh1 is inhibited by Cdk-dependent phosphorylation

(Kramer et al., 2000), and this cofactor is possibly inactive in cancer cells due to Cdk hyperactivity (Lehman et al., 2007). As shown in this work, Cdh1-deficient cells display an increased susceptibility to topoisomerase poisons (Figure 6). Overexpression of Top2α is known to correlate with susceptibility to these drugs (Figure S6; (Coutts et al., 1993; Keith et al., 1993; Smith et al., 1993), and it will be therefore interesting to test in human tumors whether Cdh1 may be useful as a biomarker for therapeutic strategies based on the use of topoisomerase poisons.

Direct inhibition of the APC/C has been recently proposed as a therapeutic strategy based on the sensitivity of the mitotic-arrested cells generated upon Cdc20 inactivation to die (Huang et al., 2009; Manchado et al., 2010b; Manchado et al., 2012). Here, we have shown that the inhibition of APC/C may have therapeutic use, not only by inhibiting Cdc20 (Manchado et al., 2010b; Zeng et al., 2010), but also by altering the levels of Cdh1 substrates. In particular, APC/C-Cdh1 inhibition by small-molecule inhibitors specifically increases Top2α levels and sensitizes cells to topoisomerase poisons. These results provide a scenario for exploring the relevance of inhibiting the APC/C with independence of its mitotic effect. Given the relevance of topoisomerase poisons in the clinic (Nitiss, 2009), these data may open avenues to explore the relevance of synthetic lethal interactions based on APC/C-Cdh1 substrates.

EXPERIMENTAL PROCEDURES

Mice and Cell Culture

Cdh1-deficient mice were reported previously (García-Higuera et al., 2008). Mice were housed in the pathogen-free animal facility of the Spanish National Cancer Research Centre (CNIO, Madrid) following the animal care standards of the institution. All animal protocols were approved by the ISCIII committee (Madrid) for animal care and research. For histological observation, dissected organs were fixed in 10%-buffered formalin (Sigma-Aldrich-Aldrich) and embedded in paraffin wax. Sections of 3 or 5 μm thickness were stained with hematoxylin and eosin (H&E). Additional immunohistochemical examination of the tissues and pathologies analyzed were performed using specific antibodies (Table S2).

MEFs were isolated from mutant and control embryos and cultured using routine procedures (García-Higuera et al., 2008). Etoposide (Sigma-Aldrich-Aldrich; 25-100 μM), ICRF-193 (Sigma-Aldrich-Aldrich, 5 μM), monastrol (Sigma-Aldrich; 100 μM), taxol (Sigma-Aldrich; 1 μM), proTAME (Boston Biochem; 10–20 μM), cycloheximide (Sigma-Aldrich; 100 μg/ml), and actinomycin D (Sigma-Aldrich; 1 μM) were used at the indicated concentrations. For quantitative RT-PCR studies, total RNA was isolated by using the QIAGEN RNeasy kit, according to the manufacturer's instructions. cDNA was synthesized with a Superscript III reverse transcriptase (Invitrogen), and PCR amplification was performed using SYBR Green PCR Master mix (Applied Biosystems) with specific primers (Table S3).

Proteomic Analysis

For SILAC analysis, equal number of asynchronous *Fzr1*(+/+) (light labeled) and *Fzr1*(–/–) (heavy labeled) mouse MEFs were mixed. For iTRAQ assays in cultured cells, primary MEFs were synchronized in G0 by confluence and low serum (0.1% FBS) for 36 hr. For iTRAQ studies in brains, E15.5 embryo brains from *Fzr1*(–/Δ)(García-Higuera et al., 2008) and control mice were lysed. Three different clones of MEFs or three different brains of each genotype were used in these assays. Protein samples were digested using the filter aided sample preparation method (Wiśniewski et al., 2009), and samples were fractionated on the basis of their isolectric point (Ernoult et al., 2008) using the 3100 OFFGEL Fractionator system (Agilent Technologies). Peptide samples were analyzed by LC-MS/MS using an LTQ Orbitrap Velos. Additional specific details are provided as Supplemental Information.

Immunoblot and Immunofluorescence

Cultured cells were lysed in RIPA or Laemmli buffer. Embryonic brains were lysed in 6 M urea, 2 M thiourea, 1% N-octyl glucoside, 10 mM DTT, 100 mM HEPES (pH 8.0) plus protease inhibitors, phosphatase inhibitors cocktail I and 2 (Sigma-Aldrich-Aldrich), and 0.1% Benzonase nuclease (Novagen). Fifty micrograms of total protein was separated by SDS-PAGE, transferred to nitrocellulose membranes (Bio-Rad), and probed with different antibodies (Table S2). The secondary antibodies were HRP-conjugated antibodies (DAKO), and the immunoblots were developed using the ECL system (PerkinElmer).

For immunofluorescence, cells were fixed in 4% buffered paraformaldehyde for 10 min at room temperature (RT), permeabilized in 0.15% Triton X-100 for 5–10 min at RT, and stained with the indicated antibodies (Table S2) and/or with 4,6 diaminophenylindole (DAPI; Prolong Gold antifade, Invitrogen) to visualize nuclei. Images were captured using a laser scanning confocal microscope TCS-SP5 (AOBS) Leica or a Leica DMI 6000B microscope. Tissues were fixed in 10%-buffered formalin (Sigma-Aldrich) and embedded in paraffin wax. Tissue sections were blocked with 3% BSA and incubated with primary antibodies (Table S2) for 1–2 hr at RT or 24 hr at 4°C. Secondary antibodies (Alexa 488, 594, or 647) from Molecular Probes (Invitrogen) were used, and images were obtained using a laser scanning confocal microscope TCS-SP5 (AOBS) Leica.

High-Throughput Microscopy and Videomicroscopy

For high-throughput microscopy (HTM), cells were grown on μCLEAR bottom 96-well plates (Greiner Bio-One). After 24 hr with etoposide and/or ICRF, 1 μM TO-PRO-3 Iodide (642/661; Invitrogen T3605) and 5 μg/ml Hoechst 33342 (Invitrogen H3570) were added. After 30 min at 37°C, images were automatically acquired from each well by an Opera High-Content Screening System (PerkinElmer). A 20× magnification lens was used, and pictures were taken at nonsaturating conditions. For videomicroscopy, cells were plated on eight-well glass-bottom dishes (Ibidi) and imaged with a DeltaVision RT imaging system (Applied Precision, LLC; IX70/71; Olympus) equipped with a Pl APO 20×/1.42 NA objective lens, maintained at 37°C in a humidified CO_2 chamber. Images were acquired every 10 min. Images were processed and analyzed using ImageJ software.

Degradation and Ubiquitination Assays

Xenopus cytostatic factor-arrested egg extracts (CSF extracts) were prepared as described previously (Murray et al., 1989). Cell-free APC/C-Cdh1-dependent assays were reconstituted by adding 280 nM purified *Xenopus* His-Cdh1 protein to interphase egg extracts (Trickey et al., 2013). To produce ^{35}S-labeled substrates, mRNAs were first synthesized using mMESSAGE mMACHINE kit (Ambion) and then translated using Rabbit Reticulocyte Lysate System (Promega).

Statistical Analysis

Statistical analysis was carried out using Prism 5 (GraphPad). All statistical tests were performed using two-sided, unpaired Student's t tests, or the Fisher's exact test. Data with $p < 0.05$ were considered statistically significant (*$p < 0.05$; **$p < 0.01$; ***$p < 0.001$).

ACCESSION NUMBERS

The mass spectrometry proteomics data have been deposited to the ProteomeXchange Consortium (http://proteomecentral.proteomexchange.org) via the PRIDE partner repository (Vizcaíno et al., 2013) under accession number PXD000511.

SUPPLEMENTAL INFORMATION

Supplemental Information includes Supplemental Experimental Procedures, seven figures, and three tables and can be found with this article online at http://dx.doi.org/10.1016/j.celrep.2014.01.017.

AUTHOR CONTRIBUTIONS

M.E., M.A.-F., and A.J.L.-C. performed most of the cellular and biochemical assays. F.G., J.L.L.-G., and J.M. performed and analyzed the proteomic analyses. K.F., H. Yaguchi, and H. Yamano performed and analyzed the assays in Xenopus. J.M., O.F.-C., H.Y., and M.M. analyzed the data and supervised the work. M.M. designed the project and wrote the manuscript.

ACKNOWLEDGMENTS

We thank Angeles Almeida, Thomas U. Mayer, William T. Beck, Anthony A. Hyman, Jan-Michael Peters, Eusebio Manchado, and Scott Lowe for reagents. M.E., A.J.L.-C., and M.A.-F. were supported by the Spanish Ministry of Education, Culture and Sports, the AECC Scientific Foundation, and the EU-PEOPLE programme, respectively. Work in the O.F.-C. laboratory was supported by grants from the Spanish Ministry of Economy and Competitiveness (MINECO; SAF2011-23753), the Association for International Cancer Research (12-0229), the Howard Hughes Medical Institute, and the European Research Council (ERC-210520). Work in the H.Y. laboratory was funded by grants from Marie Curie Cancer Care and Cancer Research UK. Work in M.M.'s laboratory was funded by grants from the Foundation Ramón Areces, MINECO (SAF2012-38215), the OncoCycle Programme (S2010/BMD-2470) from the Comunidad de Madrid, and the European Union Seventh Framework Programme (MitoSys project; HEALTH-F5-2010-241548).

Received: September 2, 2013
Revised: December 30, 2013
Accepted: January 14, 2014
Published: February 6, 2014

REFERENCES

Alchanati, I., Teicher, C., Cohen, G., Shemesh, V., Barr, H.M., Nakache, P., Ben-Avraham, D., Idelevich, A., Angel, I., Livnah, N., et al. (2009). The E3 ubiquitin-ligase Bmi1/Ring1A controls the proteasomal degradation of Top2alpha cleavage complex - a potentially new drug target. PLoS ONE *4*, e8104.

Aulia, S., and Tang, B.L. (2006). Cdh1-APC/C, cyclin B-Cdc2, and Alzheimer's disease pathology. Biochem. Biophys. Res. Commun. *339*, 1–6.

Castillo, A., Morse, H.C., 3rd, Godfrey, V.L., Naeem, R., and Justice, M.J. (2007). Overexpression of Eg5 causes genomic instability and tumor formation in mice. Cancer Res. *67*, 10138–10147.

Coutts, J., Plumb, J.A., Brown, R., and Keith, W.N. (1993). Expression of topoisomerase II alpha and beta in an adenocarcinoma cell line carrying amplified topoisomerase II alpha and retinoic acid receptor alpha genes. Br. J. Cancer *68*, 793–800.

Doménech, E., and Malumbres, M. (2013). Mitosis-targeting therapies: a troubleshooting guide. Curr. Opin. Pharmacol. *13*, 519–528.

Eguren, M., Manchado, E., and Malumbres, M. (2011). Non-mitotic functions of the Anaphase-Promoting Complex. Semin. Cell Dev. Biol. *22*, 572–578.

Eguren, M., Porlan, E., Manchado, E., García-Higuera, I., Cañamero, M., Fariñas, I., and Malumbres, M. (2013). The APC/C cofactor Cdh1 prevents replicative stress and p53-dependent cell death in neural progenitors. Nat. Commun. *4*, 2880.

Ernoult, E., Gamelin, E., and Guette, C. (2008). Improved proteome coverage by using iTRAQ labelling and peptide OFFGEL fractionation. Proteome Sci. *6*, 27.

Falnikar, A., Tole, S., and Baas, P.W. (2011). Kinesin-5, a mitotic microtubule-associated motor protein, modulates neuronal migration. Mol. Biol. Cell *22*, 1561–1574.

Ferhat, L., Cook, C., Chauviere, M., Harper, M., Kress, M., Lyons, G.E., and Baas, P.W. (1998). Expression of the mitotic motor protein Eg5 in postmitotic neurons: implications for neuronal development. J. Neurosci. *18*, 7822–7835.

García-Higuera, I., Manchado, E., Dubus, P., Cañamero, M., Méndez, J., Moreno, S., and Malumbres, M. (2008). Genomic stability and tumour suppression by the APC/C cofactor Cdh1. Nat. Cell Biol. *10*, 802–811.

Gieffers, C., Peters, B.H., Kramer, E.R., Dotti, C.G., and Peters, J.M. (1999). Expression of the CDH1-associated form of the anaphase-promoting complex in postmitotic neurons. Proc. Natl. Acad. Sci. USA *96*, 11317–11322.

Gordon, D.M., and Roof, D.M. (2001). Degradation of the kinesin Kip1p at anaphase onset is mediated by the anaphase-promoting complex and Cdc20p. Proc. Natl. Acad. Sci. USA *98*, 12515–12520.

Haque, S.A., Hasaka, T.P., Brooks, A.D., Lobanov, P.V., and Baas, P.W. (2004). Monastrol, a prototype anti-cancer drug that inhibits a mitotic kinesin, induces rapid bursts of axonal outgrowth from cultured postmitotic neurons. Cell Motil. Cytoskeleton *58*, 10–16.

Heck, M.M., Hittelman, W.N., and Earnshaw, W.C. (1988). Differential expression of DNA topoisomerases I and II during the eukaryotic cell cycle. Proc. Natl. Acad. Sci. USA *85*, 1086–1090.

Hildebrandt, E.R., and Hoyt, M.A. (2001). Cell cycle-dependent degradation of the Saccharomyces cerevisiae spindle motor Cin8p requires APC(Cdh1) and a bipartite destruction sequence. Mol. Biol. Cell *12*, 3402–3416.

Hong, K.U., Park, Y.S., Seong, Y.S., Kang, D., Bae, C.D., and Park, J. (2007). Functional importance of the anaphase-promoting complex-Cdh1-mediated degradation of TMAP/CKAP2 in regulation of spindle function and cytokinesis. Mol. Cell. Biol. *27*, 3667–3681.

Huang, H.C., Shi, J., Orth, J.D., and Mitchison, T.J. (2009). Evidence that mitotic exit is a better cancer therapeutic target than spindle assembly. Cancer Cell *16*, 347–358.

Jeng, J.C., Lin, Y.M., Lin, C.H., and Shih, H.M. (2009). Cdh1 controls the stability of TACC3. Cell Cycle *8*, 3529–3536.

Keith, W.N., Douglas, F., Wishart, G.C., McCallum, H.M., George, W.D., Kaye, S.B., and Brown, R. (1993). Co-amplification of erbB2, topoisomerase II alpha and retinoic acid receptor alpha genes in breast cancer and allelic loss at topoisomerase I on chromosome 20. Eur. J. Cancer *29A*, 1469–1475.

Konishi, Y., Stegmüller, J., Matsuda, T., Bonni, S., and Bonni, A. (2004). Cdh1-APC controls axonal growth and patterning in the mammalian brain. Science *303*, 1026–1030.

Kramer, E.R., Scheuringer, N., Podtelejnikov, A.V., Mann, M., and Peters, J.M. (2000). Mitotic regulation of the APC activator proteins CDC20 and CDH1. Mol. Biol. Cell *11*, 1555–1569.

Lehman, N.L., Tibshirani, R., Hsu, J.Y., Natkunam, Y., Harris, B.T., West, R.B., Masek, M.A., Montgomery, K., van de Rijn, M., and Jackson, P.K. (2007). Oncogenic regulators and substrates of the anaphase promoting complex/cyclosome are frequently overexpressed in malignant tumors. Am. J. Pathol. *170*, 1793–1805.

Li, M., Shin, Y.H., Hou, L., Huang, X., Wei, Z., Klann, E., and Zhang, P. (2008). The adaptor protein of the anaphase promoting complex Cdh1 is essential in maintaining replicative lifespan and in learning and memory. Nat. Cell Biol. *10*, 1083–1089.

Lin, S., Liu, M., Son, Y.J., Timothy Himes, B., Snow, D.M., Yu, W., and Baas, P.W. (2011). Inhibition of Kinesin-5, a microtubule-based motor protein, as a strategy for enhancing regeneration of adult axons. Traffic *12*, 269–286.

Malumbres, M., and Barbacid, M. (2009). Cell cycle, CDKs and cancer: a changing paradigm. Nat. Rev. Cancer *9*, 153–166.

Manchado, E., Eguren, M., and Malumbres, M. (2010a). The anaphase-promoting complex/cyclosome (APC/C): cell-cycle-dependent and -independent functions. Biochem. Soc. Trans. *38*, 65–71.

Manchado, E., Guillamot, M., de Cárcer, G., Eguren, M., Trickey, M., García-Higuera, I., Moreno, S., Yamano, H., Cañamero, M., and Malumbres, M. (2010b). Targeting mitotic exit leads to tumor regression in vivo: Modulation by Cdk1, Mastl, and the PP2A/B55α,δ phosphatase. Cancer Cell *18*, 641–654.

Manchado, E., Guillamot, M., and Malumbres, M. (2012). Killing cells by targeting mitosis. Cell Death Differ. *19*, 369–377.

Mayer, T.U., Kapoor, T.M., Haggarty, S.J., King, R.W., Schreiber, S.L., and Mitchison, T.J. (1999). Small molecule inhibitor of mitotic spindle bipolarity identified in a phenotype-based screen. Science *286*, 971–974.

Murray, A.W., Solomon, M.J., and Kirschner, M.W. (1989). The role of cyclin synthesis and degradation in the control of maturation promoting factor activity. Nature *339*, 280–286.

Myers, K.A., and Baas, P.W. (2007). Kinesin-5 regulates the growth of the axon by acting as a brake on its microtubule array. J. Cell Biol. *178*, 1081–1091.

Nadar, V.C., Ketschek, A., Myers, K.A., Gallo, G., and Baas, P.W. (2008). Kinesin-5 is essential for growth-cone turning. Curr. Biol. *18*, 1972–1977.

Nitiss, J.L. (2009). Targeting DNA topoisomerase II in cancer chemotherapy. Nat. Rev. Cancer *9*, 338–350.

Ostergaard, P., Simpson, M.A., Mendola, A., Vasudevan, P., Connell, F.C., van Impel, A., Moore, A.T., Loeys, B.L., Ghalamkarpour, A., Onoufriadis, A., et al. (2012). Mutations in KIF11 cause autosomal-dominant microcephaly variably associated with congenital lymphedema and chorioretinopathy. Am. J. Hum. Genet. *90*, 356–362.

Peters, J.M. (2006). The anaphase promoting complex/cyclosome: a machine designed to destroy. Nat. Rev. Mol. Cell Biol. *7*, 644–656.

Rath, O., and Kozielski, F. (2012). Kinesins and cancer. Nat. Rev. Cancer *12*, 527–539.

Saijo, T., Ishii, G., Ochiai, A., Yoh, K., Goto, K., Nagai, K., Kato, H., Nishiwaki, Y., and Saijo, N. (2006). Eg5 expression is closely correlated with the response of advanced non-small cell lung cancer to antimitotic agents combined with platinum chemotherapy. Lung Cancer *54*, 217–225.

Seki, A., and Fang, G. (2007). CKAP2 is a spindle-associated protein degraded by APC/C-Cdh1 during mitotic exit. J. Biol. Chem. *282*, 15103–15113.

Sigl, R., Wandke, C., Rauch, V., Kirk, J., Hunt, T., and Geley, S. (2009). Loss of the mammalian APC/C activator FZR1 shortens G1 and lengthens S phase but has little effect on exit from mitosis. J. Cell Sci. *122*, 4208–4217.

Smith, K., Houlbrook, S., Greenall, M., Carmichael, J., and Harris, A.L. (1993). Topoisomerase II alpha co-amplification with erbB2 in human primary breast cancer and breast cancer cell lines: relationship to m-AMSA and mitoxantrone sensitivity. Oncogene *8*, 933–938.

Tavormina, P.A., Côme, M.G., Hudson, J.R., Mo, Y.Y., Beck, W.T., and Gorbsky, G.J. (2002). Rapid exchange of mammalian topoisomerase II alpha at kinetochores and chromosome arms in mitosis. J. Cell Biol. *158*, 23–29.

Tiwari, V.K., Burger, L., Nikoletopoulou, V., Deogracias, R., Thakurela, S., Wirbelauer, C., Kaut, J., Terranova, R., Hoerner, L., Mielke, C., et al. (2012). Target genes of Topoisomerase IIβ regulate neuronal survival and are defined by their chromatin state. Proc. Natl. Acad. Sci. USA *109*, E934–E943.

Trickey, M., Fujimitsu, K., and Yamano, H. (2013). Anaphase-promoting complex/cyclosome-mediated proteolysis of Ams2 in the G1 phase ensures the coupling of histone gene expression to DNA replication in fission yeast. J. Biol. Chem. *288*, 928–937.

Vizcaíno, J.A., Côté, R.G., Csordas, A., Dianes, J.A., Fabregat, A., Foster, J.M., Griss, J., Alpi, E., Birim, M., Contell, J., et al. (2013). The PRoteomics IDEntifications (PRIDE) database and associated tools: status in 2013. Nucleic Acids Res. *41* (Database issue), D1063–D1069.

Watanabe, M., Tsutsui, K., Tsutsui, K., and Inoue, Y. (1994). Differential expressions of the topoisomerase II alpha and II beta mRNAs in developing rat brain. Neurosci. Res. *19*, 51–57.

Wiśniewski, J.R., Zougman, A., Nagaraj, N., and Mann, M. (2009). Universal sample preparation method for proteome analysis. Nat. Methods *6*, 359–362.

Zeng, X., Sigoillot, F., Gaur, S., Choi, S., Pfaff, K.L., Oh, D.C., Hathaway, N., Dimova, N., Cuny, G.D., and King, R.W. (2010). Pharmacologic inhibition of the anaphase-promoting complex induces a spindle checkpoint-dependent mitotic arrest in the absence of spindle damage. Cancer Cell *18*, 382–395.

Zhao, W.M., and Fang, G. (2005). Anillin is a substrate of anaphase-promoting complex/cyclosome (APC/C) that controls spatial contractility of myosin during late cytokinesis. J. Biol. Chem. *280*, 33516–33524.

Supplementary Information

A synthetic lethal interaction between APC/C and topoisomerase poisons uncovered by proteomic screens

Manuel Eguren,[1] Mónica Álvarez-Fernández,[1] Fernando García,[2] Andrés J. López-Contreras,[3] Kazuyuki Fujimitsu,[4] Hiroko Yaguchi,[4] José Luis Luque-García,[5] Oscar Fernández-Capetillo,[3] Javier Muñoz,[2] Hiroyuki Yamano[4] and Marcos Malumbres[1],*

[1] Cell Division and Cancer Group, Spanish National Cancer Research Centre (CNIO) Madrid, E-28029 Spain.

[2] Proteomics Unit, Spanish National Cancer Research Centre (CNIO) Madrid, E-28029 Spain.

[3] Genomic Instability Group, Spanish National Cancer Research Centre (CNIO) Madrid, E-28029 Spain.

[4] Cell Cycle Control Group, University College London Cancer Institute, London, WC1E 6BT U.K.

[5] Dpt. Analytical Chemistry. Complutense University of Madrid, Madrid, E-28015 Spain

Supplementary Experimental Procedures

Proteomic analysis

For SILAC (Ong et al, 2002) analysis, fifty μg of proteins were separated by SDS-PAGE, sliced into 24 pieces and digested with trypsin as described (Shevchenko et al, 2006). Desalted peptides were separated by reversed-phase chromatography (Reprosil-Pur C18 3 μm, 200x 0.075 mm, Dr. Maisch GmbH. Germany), using a nanoLCUltra1D+ system (Eksigent, Dublin CA, USA), directly coupled in line with a LTQ-Orbitrap Velos (Thermo Fisher Scientific, Waltham, USA) via nanoelectrospray source (Thermo Fisher Scientific) (Olsen et al, 2005). Mass spectra were acquired in a data-dependent manner, with an automatic switch between MS and MS/MS scans using a top 15 method. Raw files were analyzed by MaxQuant (version 1.1.1.25) (Cox and Mann, 2008) interrogating the IPI-mouse V3.77 database. Oxidation of methionines, acetylation of protein n-terminus, SILAC-K8 and SILAC-R10 were set as variable modifications, whereas carbamidomethylation of cysteines was set as fixed. Minimal peptide length was set to 6 amino acids and a maximum of two missed-cleavages were allowed. For protein assessment, at least two unique peptides with a FDR <= 1% were required. For quantification purposes, only proteins identified with two or more unique peptides and with two or more SILAC pairs were considered. For iTRAQ, (Ross et al, 2004) assays, raw files were processed by Proteome Discoverer 1.3 (Thermo Scientific). Data were searched by interrogating the Uniprot_Mouse database, comprising both the canonical and manually reviewed isoform sequences (release 2012_09, 50544 entries) using MASCOT (v 2.2) (Perkins et al., 1999) as the search engine. Lysine and peptide N-termini labelling with iTRAQ-4plex reagent as well as carbamidomethylation of cysteine were considered as fixed modifications, while oxidation of methionine was chosen as variable modification for database searching. Both peptide and protein identification were filtered at 1% false discovery rate (FDR) using the target-decoy approach (Elias and Gygi, 2007). The thresholds used to determine proteins being up-regulated were calculated by manual inspection of the data. To this end, ratios were plotted against intensities and a cut-off was chosen based on the distribution of the vast majority of proteins showing no change for each the three analyses. The narrower distributions of the iTRAQ-labelled experiments are due to the compression of ratios associated with this technique.

Supplementary Figures

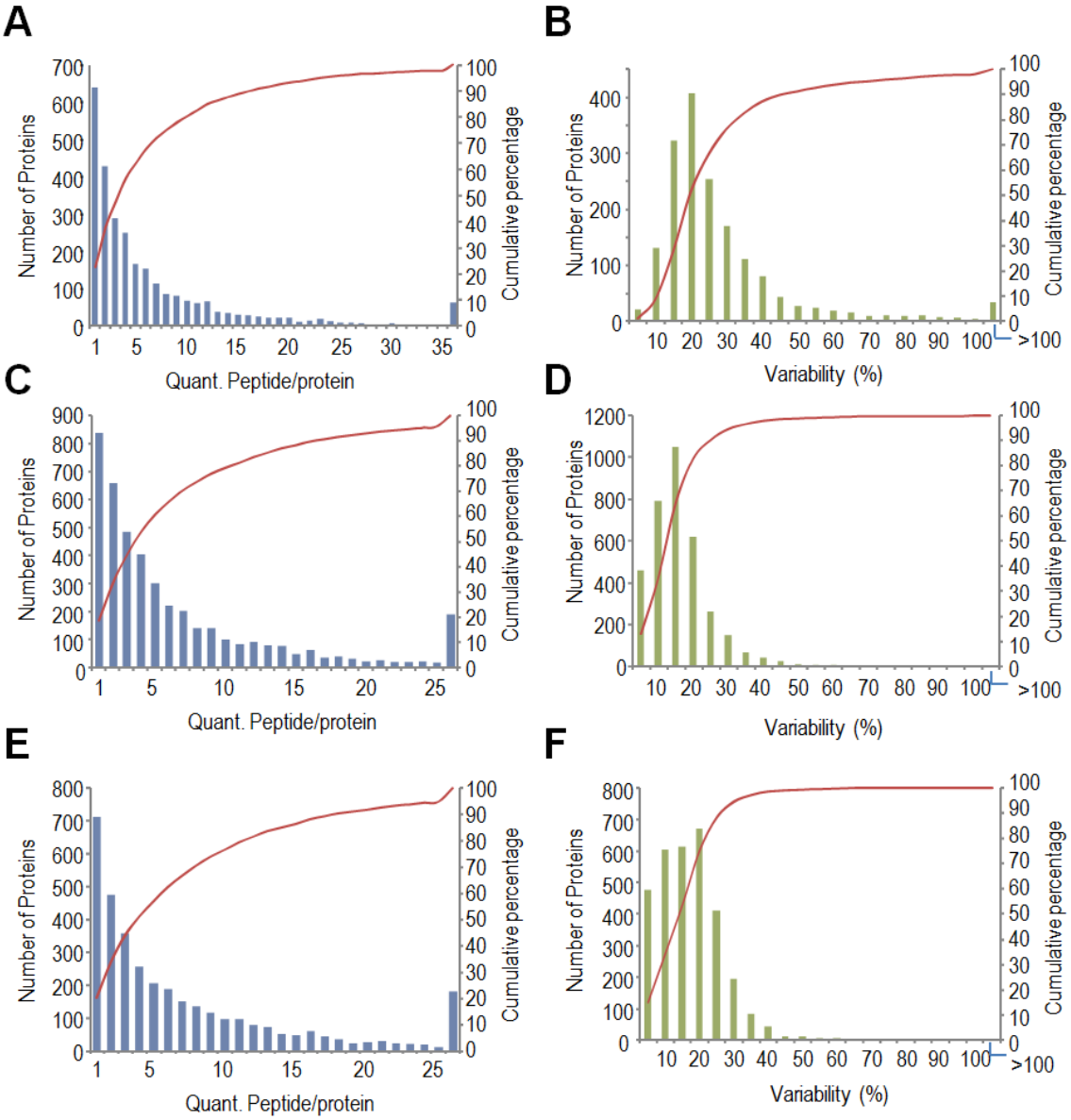

Figure S1. Evaluation of protein quantification quality in the three proteomic screenings (related to Figs. 1 and 2). The number of quantified peptides per protein is shown for A, SILAC-labeled MEFs, C, iTRAQ-labeled serum-starved MEFs and E, iTRAQ-labeled Cdh1-brains. In all three cases, more than 80% of the proteins were quantified on the basis of at least 2 unique peptides. Furthermore, 76-95% of the quantified proteins showed variability levels (i.e. relative standard deviation, RSD) below 30% for B, SILAC-labeled MEFs, D, iTRAQ-labeled serum-starved MEFs and F, iTRAQ-labeled Cdh1-deficient brains.

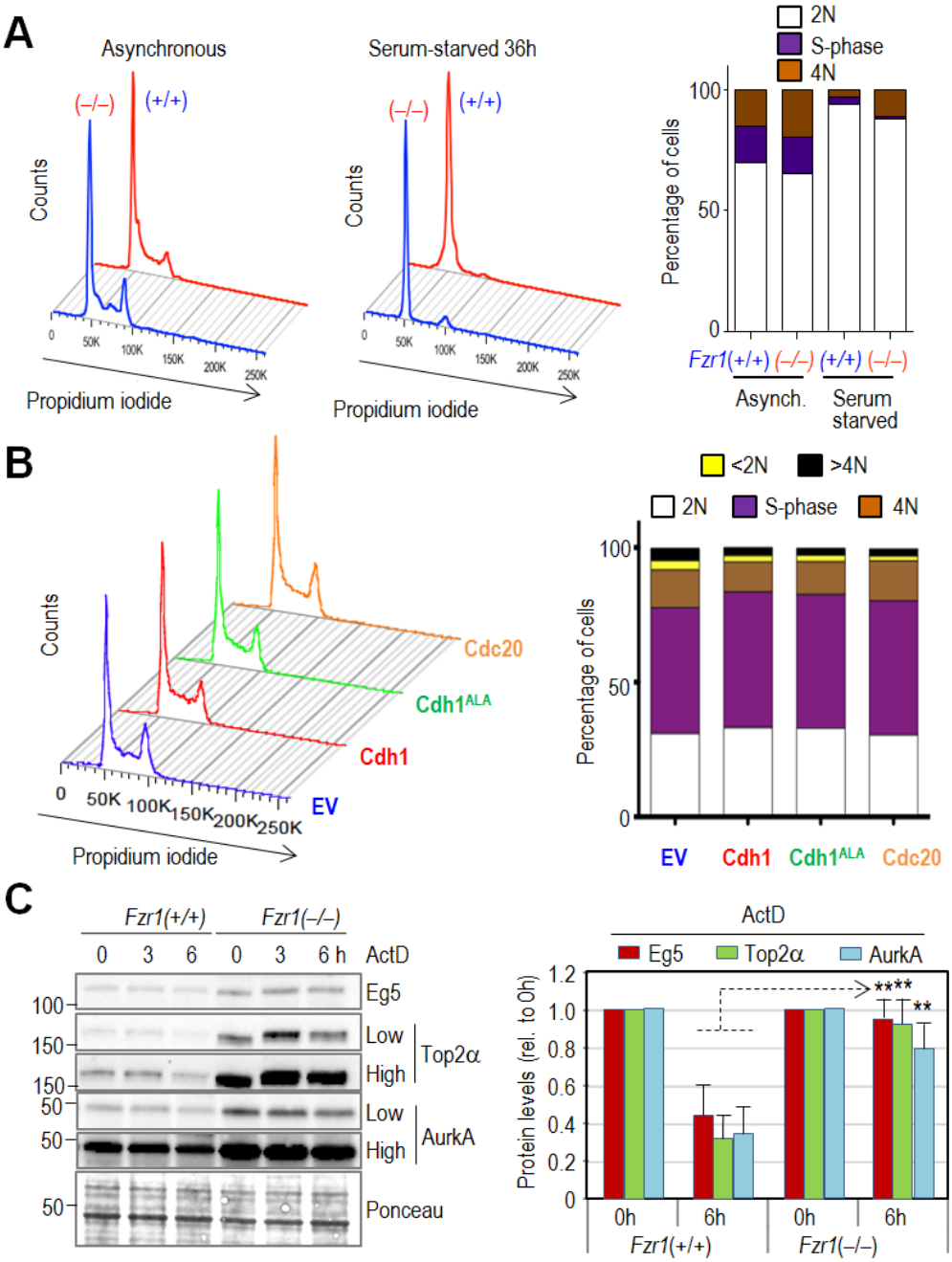

Figure S2. Cell Cycle profiles of cells deficient or overexpressing Cdh1 and stability of substrates upon treatment with actinomycin D (Related to Figs. 1-3). A, Cell cycle profiles of Cdh1-wild-type or Cdh1-null cells in the conditions used for the proteomic analysis. Note that Cdh1-null cells usually display increased 4N content due to the presence of tetraploid/binucleated cells. Histogram indicates representative average percentage of 2N cells (G0/G1), intermediate 2N-4N content (S-phase) or 4N (G2/M or tetraploid). B, Cell cycle profile of 293T cells after the expression of the indicated proteins or the empty vector (EV). The histogram represents the quantification of the percentage of cells in the different phases of the cell cycle in the previous assay. C, Protein stability of the indicated molecules in the presence of Actinomycin D (ActD) in Cdh1-null and control cells. Signals after low or high exposure are indicated for Aurora A and Top2α. The quantification of protein levels at 0 and 6 h after the addition of ActD is shown in the histogram. Data indicate mean ± SEM in two separate assays. **, p<0.01, Student's t-test.

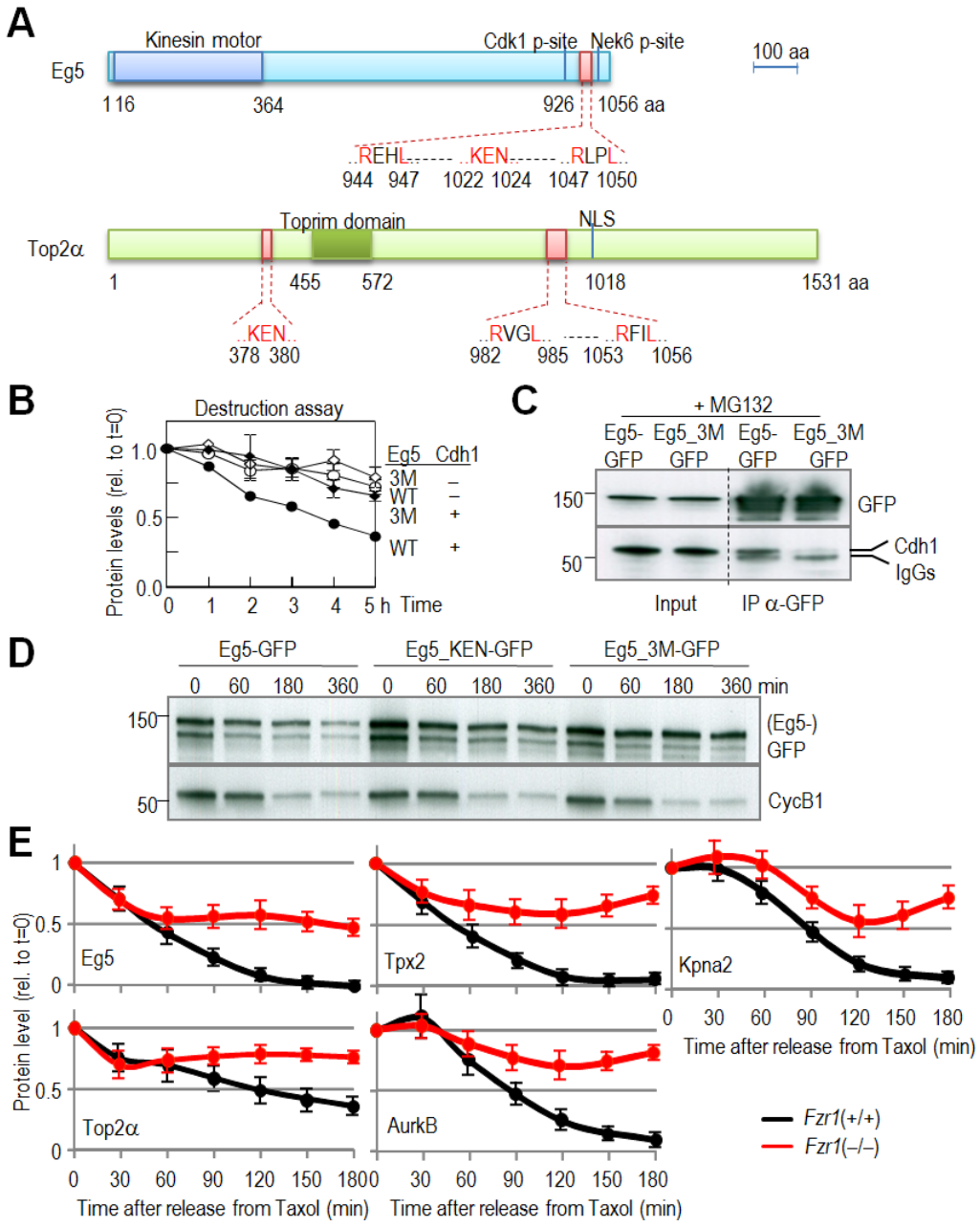

Figure S3. KEN and D-boxes in Eg5 and Top2α and kinetics of substrates in Cdh1-null cells. (related to Figs. 3-4) A, Schematic representation of human Eg5 and Top2α domains including putative KEN and D-boxes. Residues in red were mutated to alanine to generate stable proteins (3M mutants). B, Quantification of the destruction assay in Fig. 3H. Both the upper and lower (likely a prematurely terminated or partly cleaved product) bands in Fig. 3H show a similar kinetics. Only the upper band is quantified in the plot. Error bars, SEM from three independent experiments. C, Co-immunoprecipitation studies in 293T cells expressing Eg5-GFP or Eg5_3M-GFP fusion proteins. Protein extracts were immunoprecipitated with antibodies against GFP and the endogenous Cdh1 was detected in the presence of the proteasome inhibitor MG132. D, Protein levels of the exogenous Eg5-GFP fusion protein at different time points after a release from nocodazole. Eg5-KEN-GFP is mutated in the KEN box whereas Eg5_3M-GFP contains mutations in the KEN and two putative D-boxes. E, Comparative quantification of the levels of the indicated proteins after release from taxol in Cdh1-null [*Fzr1*(–/–)] or control [*Fzr1*(+/+)] MEFS. Values (mean ± SEM) were normalized to the amount of protein at t=0 (in the presence of taxol).

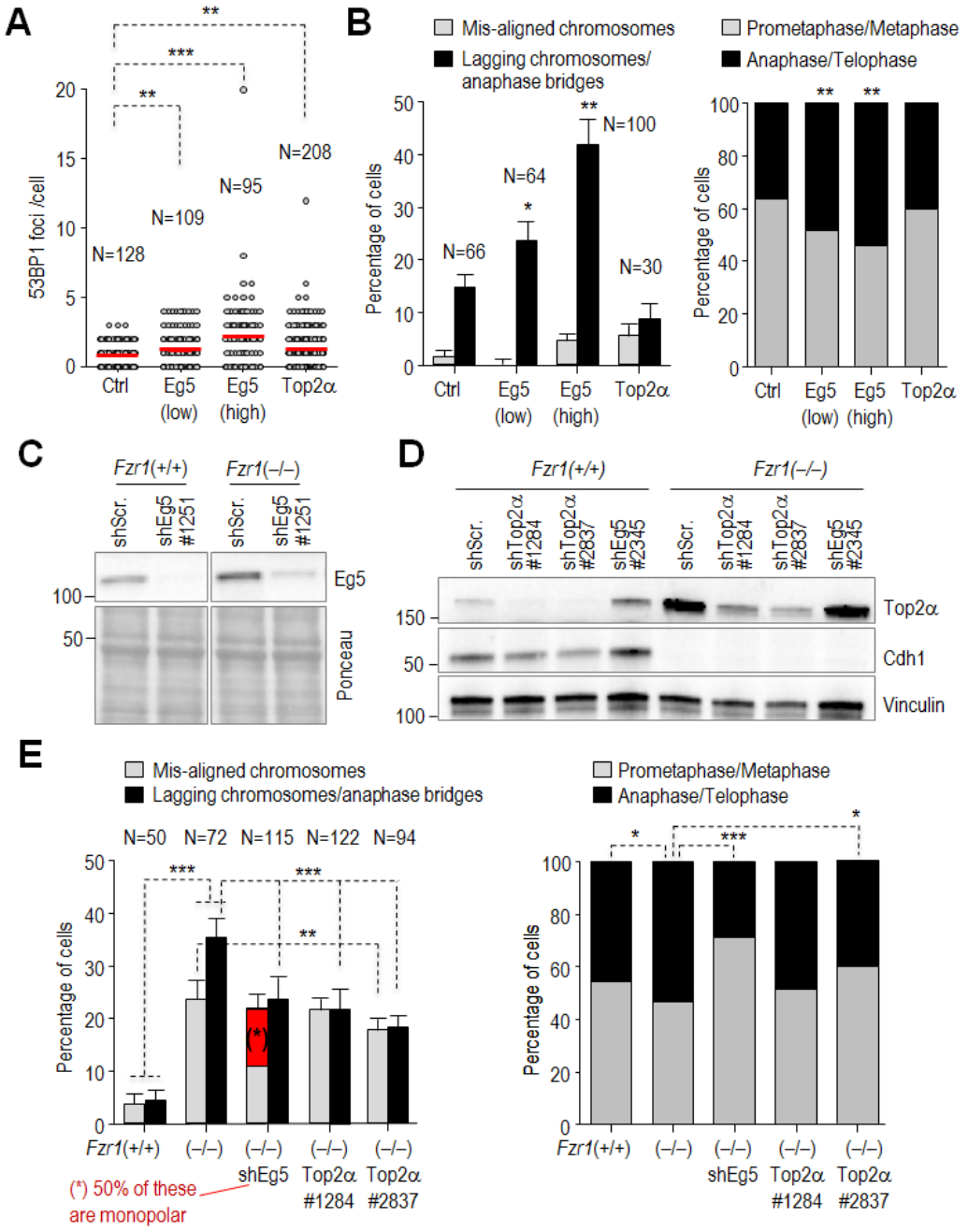

Figure S4. Effect of Eg5 and Top2α levels in genomic instability (related to Fig. 4). A, U2OS cells were transfected with Eg5 (low or high concentration) or Top2α and the number of 53BP1 foci was scored by immunofluorescence. Means are indicated by a red bar. N, number of cells. B, Mitotic aberrations were scored by immunofluorescence with antibodies against α-tubulin and DAPI to stain DNA. Data represent percentage of mitotic cells (mean ± SEM in three experiments). C-D, Downregulation of endogenous Eg5 (C) or Top2α (D) after transfection of Cdh1-null [*Fzr1*(–/–)] or control [*Fzr1*(+/+)] MEFs with short hairpin interfering RNAs (shRNAs) against these molecules. E, Mitotic aberrations (mean ± SEM in three experiments) in wild-type or Cdh1-null cells after knock-down of Eg5 or Top2α with the indicated shRNAs. N, number of cells. *, p<0.05; **, p<0.01; ***, p<0.001 (Student's t-test).

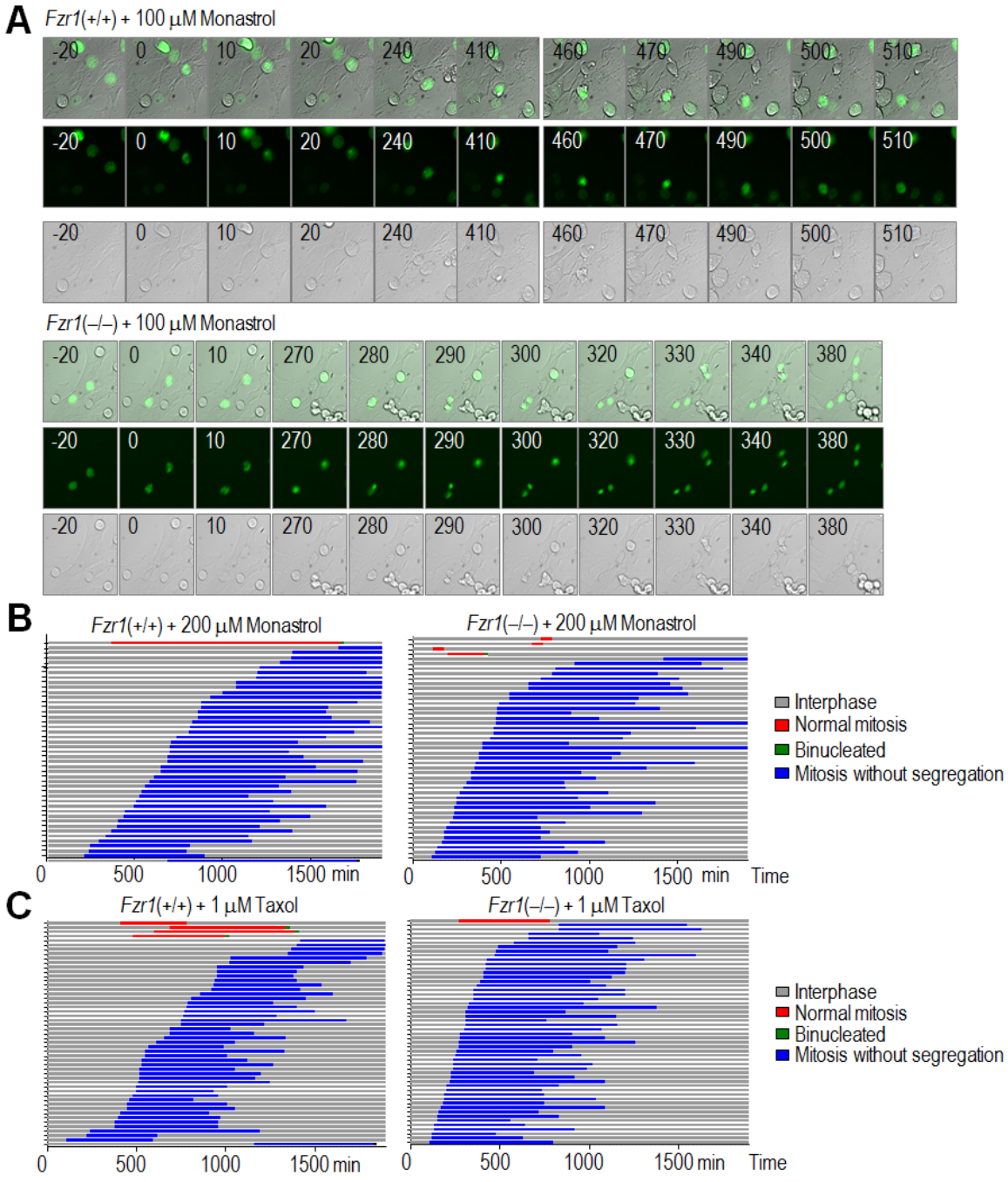

Figure S5. Effect of monastrol or taxol in Cdh1-null [*Fzr1*(–/–)] or wild-type [*Fzr1*(+/+)] cells (related to Fig. 5). A, Extended version from Figure 6B. Scale bars, 10 μM. B, Effect of increased (200 μM) dose of monastrol in wild-type or Cdh1-null cells, showing that the resistance of Cdh1-null cells to monastrol is dose-dependent. C, Effect of taxol in wild-type and Cdh1-null cells showing that lack of Cdh1 does not result in resistance to this microtubule poison.

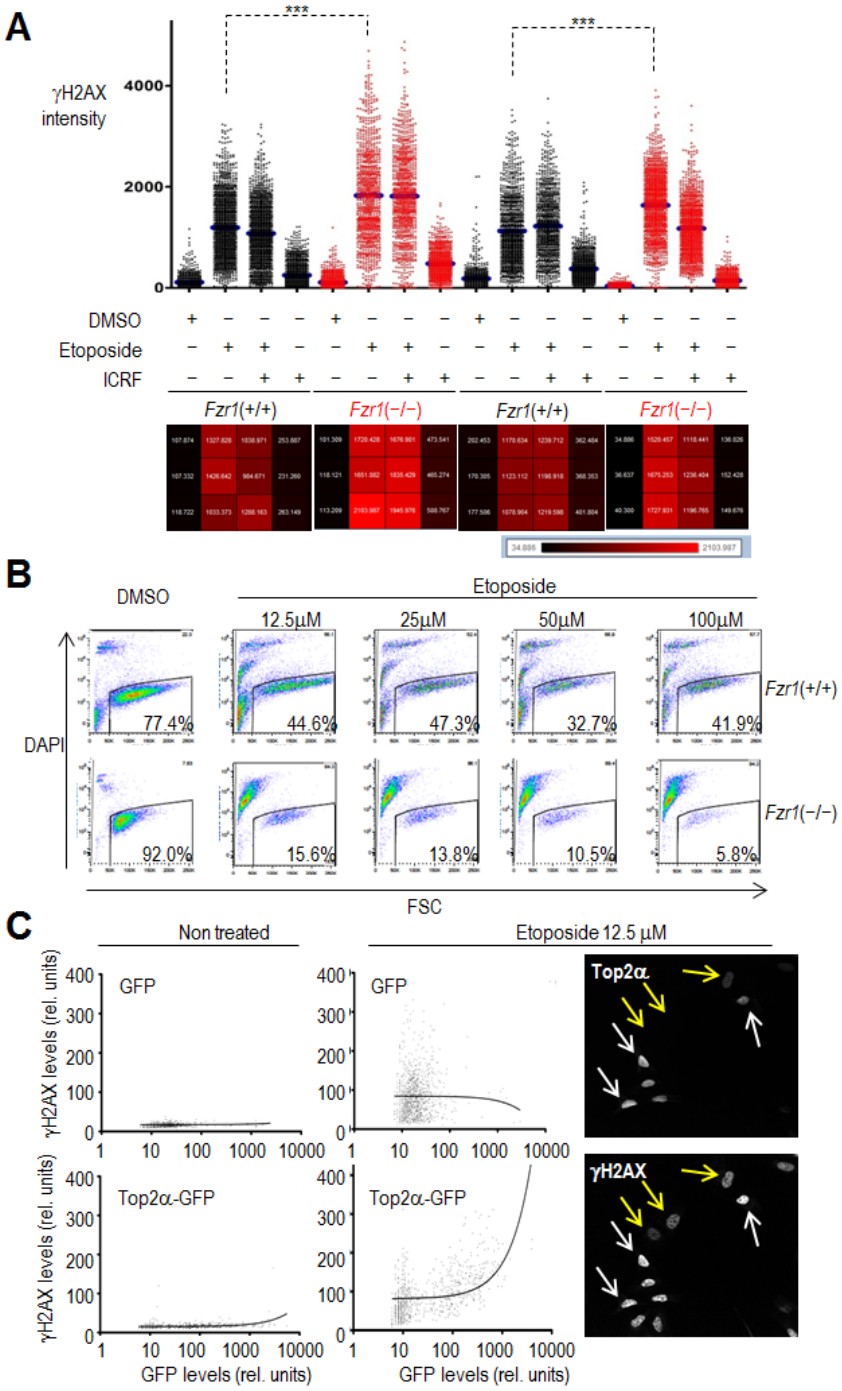

Figure S6. Effect of etoposide in Cdh1-null and control cells (related to Fig. 6). A, Quantification of phosphorylation of H2AX (γH2AX intensity per cell) after treatment of Cdh1-null or control cells with etoposide or ICRF-193. Please note that etoposide and ICRF-193 were added at the same time and, in these conditions, the addition of ICRF-193 is not efficient in preventing DNA damage induced by etoposide. B, Quantification of the lethal effect of etoposide at the indicated doses in Cdh1-null or control cells. The percentage of live cells (negative for DAPI) is indicated in each condition. Data show a representative assay of three independent experiments. C, γH2AX intensity per cell after overexpression of GFP or Top2α-GFP, in the absence or presence of the indicated dose of etoposide. Lines indicate regression analysis of the data. Pictures on the right represent levels of γH2AX in cells positive (white arrows) or negative (yellow arrows) for Top2α overexpression.

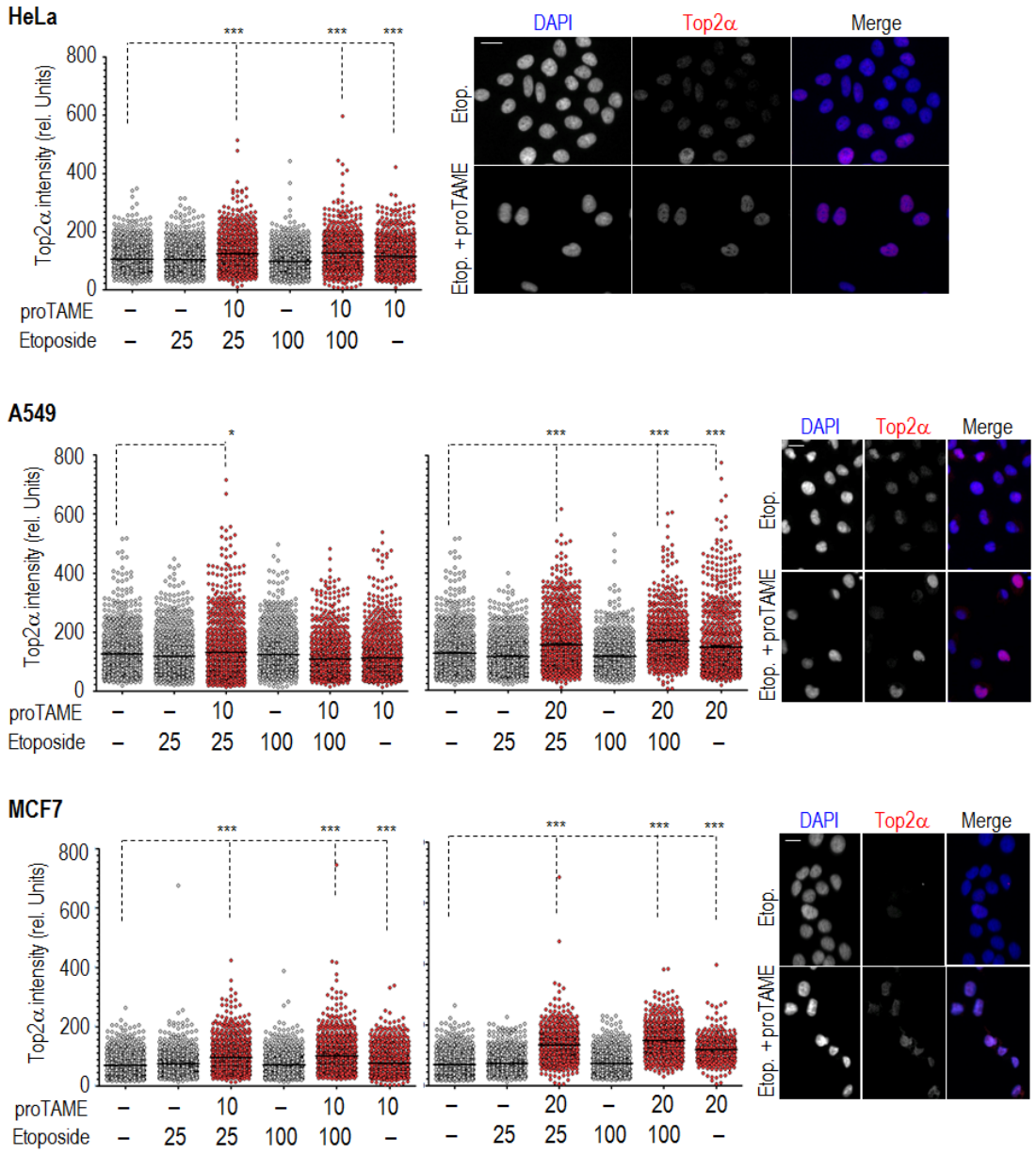

Figure S7. Protein levels of Top2α after inhibition of the APC/C in human cell lines (related to Fig. 7). Quantification of Top2α levels in HeLa, A549 or MCF7 cells treated with the indicated dose of proTAME or etoposide (μM). Representative images of cells treated with 25 μM etoposide or 25 μM etoposide + 10 μM proTAME (HeLa) or 25 μM etoposide + 20 μM proTAME (A549 and MCF7) are shown. Top2α is in red and DAPI in blue. Scale bars, 10 μM. At least 4000 cells per condition were quantified in these assays and only 1000 are represented in the plots for clarity. ***, $p<0.001$; Student's t-test.

Supplementary Tables

Table S1. Known APC/C substrates identified in our work (related to Table 1 and Figs 1-2).

Symbol	Uniprot	Description	Asynchr. Log*	G0 Log*	Brains Log*	Reference
Anln	Q8K298	Actin-binding protein anillin	1.668	0.983	nd	(Zhao & Fang, 2005)
Aurka	P97477	Aurora kinase A	nd	0.225	nd	(Taguchi et al, 2002) (Littlepage & Ruderman, 2002)
Aurkb	O70126	Aurora kinase B	0.991	nd	2.355	(Stewart & Fang, 2005) (Nguyen et al, 2005)
Brsk2	Q69Z98	Serine/threonine-protein kinase BRSK2	nd	nd	0.188	(Li et al, 2012)
Ccna2	P51943	Cyclin-A2	nd	-0.44	nd	(den Elzen & Pines, 2001) (Geley et al, 2001)
Ccnb1	P24860	Ccnb1 protein	nd	0.136	nd	(Clute & Pines, 1999)
Cdk5	P49615	Cyclin-dependent kinase 5	nd	0.085	-0.03	(Zhang et al, 2012)
Ckap2	Q3V1H1	Cytoskeleton-associated protein 2	2.116	1.024	0.845	(Seki & Fang, 2007) (Hong et al, 2007)
Dnmt1	P13864	DNA (cytosine-5)-methyltransferase 1	nd	0.03	-0.18	(Ghoshal et al, 2005)
Fan1	Q69ZT1	Fanconi-associated nuclease 1	-0.15	nd	nd	(Lai et al, 2012)
FoxM1	O08696	Forkhead box protein M1	nd	nd	-0.05	(Park et al, 2008)
Gls	D3Z7P3-2	Isoform 2 of Glutaminase kidney isoform, mitochondrial	nd	-0.37	-0.28	(Colombo et al, 2011)
Gtse1	Q8R080	G2 and S phase-expressed protein 1	nd	0.794	nd	(Pfleger & Kirschner, 2000)
Hmmr	Q00547	Hyaluronan mediated motility receptor	0.27	nd	nd	(Song & Rape, 2010)
Iqgap1	Q9JKF1	Ras GTPase-activating-like protein IQGAP1	0.877	-0.01	-0.19	(Ko et al, 2007)
Kif22	Q3V300	Kinesin-like protein KIF22	1.322	nd	nd	(Feine et al, 2007)
Mapk9	Q9WTU6	Isoform Alpha-1 of Mitogen-activated protein kinase 9	nd	-0.07	nd	(Gutierrez et al, 2010)
Mcl1	P97287	Induced myeloid leukemia cell differentiation protein Mcl-1 homolog	nd	-0.06	nd	(Harley et al, 2010)
RacGAP1	Q9WVM1	Rac GTPase-activating protein 1	0.33	nd	nd	(Nishimura et al, 2013)
Ndc80	Q9D0F1	Kinetochore protein NDC80 homolog	nd	nd	0.654	(Li et al, 2011)
Neurod2	Q62414	Neurogenic differentiation factor 2	nd	nd	-0.24	(Yang et al, 2009)
Nusap1	Q9ERH4	Nucleolar and spindle-associated	nd	nd	2.377	(Song & Rape,

		protein 1				2010)
Rrm2	P11157	Ribonucleoside-diphosphate reductase subunit M2	nd	0.255	-0.08	(Chabes et al, 2003)
Skp2	Q9Z0Z3	S-phase kinase-associated protein 2	nd	nd	0.283	(Bashir et al, 2004)(Wei et al, 2004)
Tacc3	Q9JJ11	Transforming acidic coiled-coil-containing protein 3	nd	0.845	1.959	(Jeng et al, 2009)
Tpx2	A2APB8	Targeting protein for Xklp2	0.623	nd	nd	(Stewart & Fang, 2005)
Trrap	Q80YV3	Transformation/transcription domain-associated protein	-0.04	-0.01	0.07	(Ichim et al, 2013)
Ube2c	Q9D1C1	Ubiquitin-conjugating enzyme E2 C	nd	0.041	nd	(Williamson et al, 2009)
Ube2s	Q921J4	Ubiquitin-conjugating enzyme E2 S	1.59	0.11	nd	(Williamson et al, 2009)

* nd, not detected.

Table S2. Antibodies used in this work (related to Figs. 1-4,6,7,S2,S3,S4,S6,S8).

Antigen	Ig	Source	Clone	Cat Number	Dilution	Technique*
53BP1	Rabbit	Novus Biologicals		NB100-304	1:1000	IF
AurkA	Mouse	Becton Dickinson	4/IAK1	610938	1:25	IHC
AurkA	Mouse	Abcam		ab13824	1:500	WB
AurkB	Rabbit	Abcam		ab2254	1:100-1:200	IHC/WB
β-Catenin	Mouse	Sigma		C 7207	1:1500	WB
Cdc20/p55CDC	Rabbit	Santa Cruz Biotechnology		sc-8358	1:200	WB
Cdc27	Mouse	Abcam		ab10538	1:500	WB
Cdh1	Mouse	Neomarkers	CH01	MS-1116-P	1:200	WB
Cyclin B1	Mouse	Chemicon		MAB3684	1:1000	WB
Gapdh	Mouse	Sigma		G9545	1:10000	WB
GFP	Mouse	Roche		11814460001	1:2000	WB
Kif11/Eg5	Rabbit	Cytoskeleton		AKIN03	1:500-1:1000	WB/IF
Kpna2	Rabbit	Novus			1:500	WB
Phospho-Histone H2A.X (Ser139)	Mouse	Millipore	JBW301	05-636	1:1000	IF
Rock2	Rabbit	Santa Cruz Biotechnology	H-85	sc-5561	1:200	WB
Securin	Mouse	Abcam		ab3305	1:500	WB
Skp1 p19	Rabbit	Santa Cruz Biotechnology	H-163	sc-7163	1:200	WB
Top2α	Rabbit	TopoGEN		2011-1	1:500-1:1000	WB/IF
Tpx2	Rabbit	Lifespan Biosciences		LS-B146	1:250-1:1000	IHC, WB
	Rabbit	Hyman's lab (MPI-CBG)			1:500	IF
	Mouse	Abcam		ab32795	1:500	WB
Vinculin	Mouse	Sigma-Aldrich	hVIN1	V9131	1:3000	WB

* IF, Immunofluorescence; IHC, immunohistochemistry; WB, immunoblot

Table S3. Oligonucleotides used in this work against mouse sequences (related to Fig. 3).

Primer	Sequence
Top2α_Forward	5′ TGGTCAGTTTGGAACCAGGC 3′
Top2α_Reverse	5′ TCAGGCTCAACACGTTGGTT 3′
Kif11_Forward	5′ TGGCAGTGCGAAACAAAAGG 3′
Kif11_Reverse	5′ TCTGAGAAACACGAGCGGAC 3′
Gadd45a_Forward	5' GCTCAACGTAGACCCCGATA 3'
Gadd45a_Reverse	5' GTTCGTCACCAGCACACAGT 3'
Cdkn1a_Forward	5' GTGGGTCTGACTCCAGCCC 3'
Cdkn1a_Reverse	5' CCTTCTCGTGAGACGCTTAC 3'
Tpx2_Forward	5' CCTCACAGATGAGCGAATCA 3'
Tpx2_Reverse	5' TCTTCCCTTTGGACAGGTTG 3'
Gapdh_Forward	5' GCCACCCAGAAGACTGTGGATGGC 3'
Gapdh_Reverse	5' CATGATGGCCATGAGGTCCACCAC 3'

Supplementary References

Bashir T, Dorrello NV, Amador V, Guardavaccaro D, Pagano M (2004) Control of the SCF(Skp2-Cks1) ubiquitin ligase by the APC/C(Cdh1) ubiquitin ligase. *Nature* 428: 190-193

Clute P, Pines J (1999) Temporal and spatial control of cyclin B1 destruction in metaphase. *Nat Cell Biol* 1: 82-87

Colombo SL, Palacios-Callender M, Frakich N, Carcamo S, Kovacs I, Tudzarova S, Moncada S (2011) Molecular basis for the differential use of glucose and glutamine in cell proliferation as revealed by synchronized HeLa cells. *Proc Natl Acad Sci U S A* 108: 21069-21074

Chabes AL, Pfleger CM, Kirschner MW, Thelander L (2003) Mouse ribonucleotide reductase R2 protein: a new target for anaphase-promoting complex-Cdh1-mediated proteolysis. *Proc Natl Acad Sci U S A* 100: 3925-3929

den Elzen N, Pines J (2001) Cyclin A is destroyed in prometaphase and can delay chromosome alignment and anaphase. *J Cell Biol* 153: 121-136

Feine O, Zur A, Mahbubani H, Brandeis M (2007) Human Kid is degraded by the APC/C(Cdh1) but not by the APC/C(Cdc20). *Cell Cycle* 6: 2516-2523

Geley S, Kramer E, Gieffers C, Gannon J, Peters JM, Hunt T (2001) Anaphase-promoting complex/cyclosome-dependent proteolysis of human cyclin A starts at the beginning of mitosis and is not subject to the spindle assembly checkpoint. *J Cell Biol* 153: 137-148

Ghoshal K, Datta J, Majumder S, Bai S, Kutay H, Motiwala T, Jacob ST (2005) 5-Aza-deoxycytidine induces selective degradation of DNA methyltransferase 1 by a proteasomal pathway that requires the KEN box, bromo-adjacent homology domain, and nuclear localization signal. *Mol Cell Biol* 25: 4727-4741

Gutierrez GJ, Tsuji T, Chen M, Jiang W, Ronai ZA (2010) Interplay between Cdh1 and JNK activity during the cell cycle. *Nat Cell Biol* 12: 686-695

Harley ME, Allan LA, Sanderson HS, Clarke PR (2010) Phosphorylation of Mcl-1 by CDK1-cyclin B1 initiates its Cdc20-dependent destruction during mitotic arrest. *EMBO J* 29: 2407-2420

Hong KU, Park YS, Seong YS, Kang D, Bae CD, Park J (2007) Functional importance of the anaphase-promoting complex-Cdh1-mediated degradation of TMAP/CKAP2 in regulation of spindle function and cytokinesis. *Mol Cell Biol* 27: 3667-3681

Ichim G, Mola M, Finkbeiner MG, Cros MP, Herceg Z, Hernandez-Vargas H (2013) The histone acetyltransferase component TRRAP is targeted for destruction during the cell cycle. *Oncogene*

Jeng JC, Lin YM, Lin CH, Shih HM (2009) Cdh1 controls the stability of TACC3. *Cell Cycle* 8: 3529-3536

Ko N, Nishihama R, Tully GH, Ostapenko D, Solomon MJ, Morgan DO, Pringle JR (2007) Identification of yeast IQGAP (Iqg1p) as an anaphase-promoting-complex substrate and its role in actomyosin-ring-independent cytokinesis. *Mol Biol Cell* 18: 5139-5153

Lai F, Hu K, Wu Y, Tang J, Sang Y, Cao J, Kang T (2012) Human KIAA1018/FAN1 nuclease is a new mitotic substrate of APC/C(Cdh1). *Chin J Cancer* 31: 440-448

Li L, Zhou Y, Wang GF, Liao SC, Ke YB, Wu W, Li XH, Zhang RL, Fu YC (2011) Anaphase-promoting complex/cyclosome controls HEC1 stability. *Cell Prolif* 44: 1-9

Li R, Wan B, Zhou J, Wang Y, Luo T, Gu X, Chen F, Yu L (2012) APC/C(Cdh1) targets brain-specific kinase 2 (BRSK2) for degradation via the ubiquitin-proteasome pathway. *PLoS One* 7: e45932

Littlepage LE, Ruderman JV (2002) Identification of a new APC/C recognition domain, the A box, which is required for the Cdh1-dependent destruction of the kinase Aurora-A during mitotic exit. *Genes Dev* 16: 2274-2285

Nguyen HG, Chinnappan D, Urano T, Ravid K (2005) Mechanism of Aurora-B degradation and its dependency on intact KEN and A-boxes: identification of an aneuploidy-promoting property. *Mol Cell Biol* 25: 4977-4992

Nishimura K, Oki T, Kitaura J, Kuninaka S, Saya H, Sakaue-Sawano A, Miyawaki A, Kitamura T (2013) APC(CDH1) targets MgcRacGAP for destruction in the late M phase. *PLoS One* 8: e63001

Olsen JV, de Godoy LM, Li G, Macek B, Mortensen P, Pesch R, Makarov A, Lange O, Horning S, Mann M (2005) Parts per million mass accuracy on an Orbitrap mass spectrometer via lock mass injection into a C-trap. *Mol Cell Proteomics* 4: 2010-2021

Ong SE, Blagoev B, Kratchmarova I, Kristensen DB, Steen H, Pandey A, Mann M (2002) Stable isotope labeling by amino acids in cell culture, SILAC, as a simple and accurate approach to expression proteomics. *Mol Cell Proteomics* 1: 376-386

Park HJ, Costa RH, Lau LF, Tyner AL, Raychaudhuri P (2008) Anaphase-promoting complex/cyclosome-CDH1-mediated proteolysis of the forkhead box M1 transcription factor is critical for regulated entry into S phase. *Mol Cell Biol* 28: 5162-5171

Pfleger CM, Kirschner MW (2000) The KEN box: an APC recognition signal distinct from the D box targeted by Cdh1. *Genes Dev* 14: 655-665

Ross PL, Huang YN, Marchese JN, Williamson B, Parker K, Hattan S, Khainovski N, Pillai S, Dey S, Daniels S, Purkayastha S, Juhasz P, Martin S, Bartlet-Jones M, He F, Jacobson A, Pappin DJ (2004) Multiplexed protein quantitation in Saccharomyces cerevisiae using amine-reactive isobaric tagging reagents. *Mol Cell Proteomics* 3: 1154-1169

Seki A, Fang G (2007) CKAP2 is a spindle-associated protein degraded by APC/C-Cdh1 during mitotic exit. *J Biol Chem* 282: 15103-15113

Shevchenko A, Tomas H, Havlis J, Olsen JV, Mann M (2006) In-gel digestion for mass spectrometric characterization of proteins and proteomes. *Nat Protoc* 1: 2856-2860

Song L, Rape M (2010) Regulated degradation of spindle assembly factors by the anaphase-promoting complex. *Mol Cell* 38: 369-382

Stewart S, Fang G (2005) Anaphase-promoting complex/cyclosome controls the stability of TPX2 during mitotic exit. *Mol Cell Biol* 25: 10516-10527

Taguchi S, Honda K, Sugiura K, Yamaguchi A, Furukawa K, Urano T (2002) Degradation of human Aurora-A protein kinase is mediated by hCdh1. *FEBS Lett* 519: 59-65

Wei W, Ayad NG, Wan Y, Zhang GJ, Kirschner MW, Kaelin WG, Jr. (2004) Degradation of the SCF component Skp2 in cell-cycle phase G1 by the anaphase-promoting complex. *Nature* 428: 194-198

Williamson A, Wickliffe KE, Mellone BG, Song L, Karpen GH, Rape M (2009) Identification of a physiological E2 module for the human anaphase-promoting complex. *Proc Natl Acad Sci U S A* 106: 18213-18218

Yang Y, Kim AH, Yamada T, Wu B, Bilimoria PM, Ikeuchi Y, de la Iglesia N, Shen J, Bonni A (2009) A Cdc20-APC ubiquitin signaling pathway regulates presynaptic differentiation. *Science* 326: 575-578

Zhang J, Li H, Zhou T, Zhou J, Herrup K (2012) Cdk5 levels oscillate during the neuronal cell cycle: Cdh1 ubiquitination triggers proteosome-dependent degradation during S-phase. *J Biol Chem* 287: 25985-25994

Zhao WM, Fang G (2005) Anillin is a substrate of anaphase-promoting complex/cyclosome (APC/C) that controls spatial contractility of myosin during late cytokinesis. *J Biol Chem* 280: 33516-33524